ABL kinases regulate translation in HER2+ cells through Y-box-binding protein 1 to facilitate colonization of the brain

Courtney M. McKernan[1], Aaditya Khatri[1,2], Molly Hannigan[3], Jessica Child[3], Qiang Chen[3], Benjamin Mayro[1], David Snyder[4], Christopher V. Nicchitta[3], Ann Marie Pendergast[1,5,*]

[1]Department of Pharmacology and Cancer Biology, Duke University School of Medicine, Durham, NC 27710, USA

[2]Department of Medicine, Duke University School of Medicine, Durham, NC 27710, USA

[3]Department of Cell Biology, Duke University School of Medicine, Durham, NC 27710, USA

[4]Department of Surgery, Duke University School of Medicine, Durham, NC 27710, USA

[5]Lead contact

SUMMARY

Patients with human epidermal growth factor receptor 2-positive (HER2+/ERBB2) breast cancer often present with brain metastasis. HER2-targeted therapies have not been successful to treat brain metastases in part due to poor blood-brain barrier (BBB) penetrance and emergence of resistance. Here, we report that Abelson (ABL) kinase allosteric inhibitors improve overall survival and impair HER2+ brain metastatic outgrowth *in vivo*. Mechanistically, ABL kinases phosphorylate the RNA-binding protein Y-box-binding protein 1 (YB-1). ABL kinase inhibition disrupts binding of YB-1 to the *ERBB2* mRNA and impairs translation, leading to a profound decrease in HER2 protein levels. ABL-dependent tyrosine phosphorylation of YB-1 promotes HER2 translation. Notably, loss of YB-1 inhibits brain metastatic outgrowth and impairs expression of a subset of ABL-dependent brain metastatic targets. These data support a role for ABL kinases in the translational regulation of brain metastatic targets through YB-1 and offer a therapeutic target for HER2+ brain metastasis patients.

In brief

HER2 is upregulated in brain metastases and promotes outgrowth in the brain parenchyma. Here, McKernan et al. identify an ABL-YB-1 signaling axis that regulates translation of *ERBB2* and

other metastatic targets and reveal that inhibition of this pathway decreases colonization and improves overall survival in mouse models of brain metastasis.

Graphical Abstract
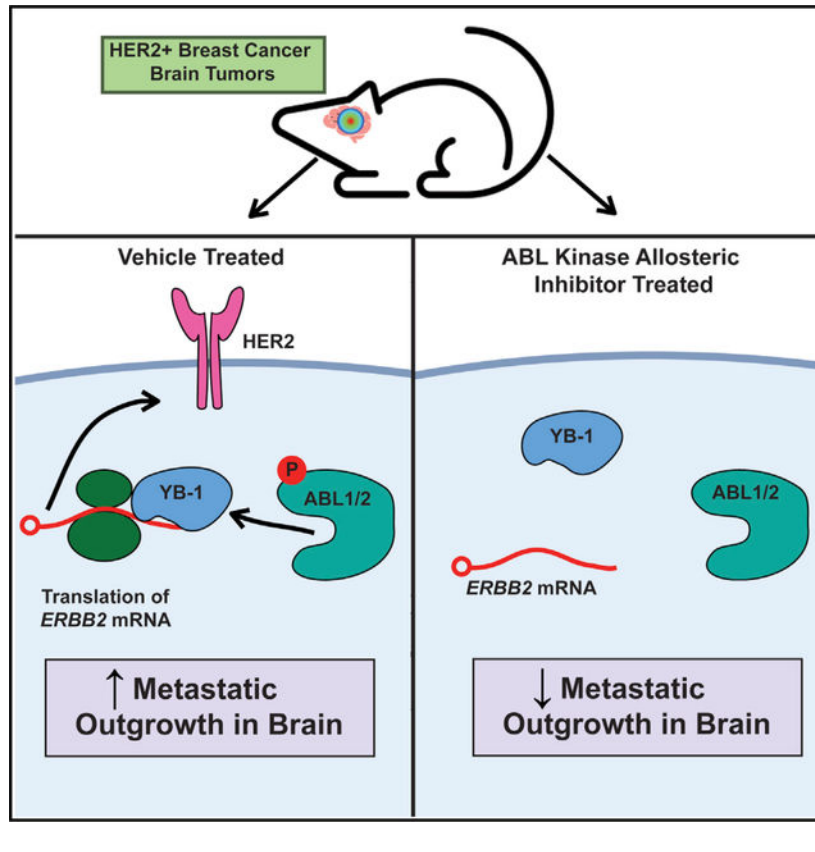
INTRODUCTION

Brain metastasis is a devastating complication among patients with late-stage breast cancer with a median survival of 8.7 months from the time of diagnosis and limited therapeutic options (Niikura et al., 2014). Patients with breast cancer brain metastasis (BCBM) experience cognitive impairment, seizures, and cranial neuropathies, leading to an overall decrease in quality of life (Rostami et al., 2016). Human epidermal growth factor receptor 2-positive (HER2+/ERBB2) breast cancer accounts for 20%–30% of all patients with breast cancer, and approximately 45% of these patients present with BCBM (Pauletti et al., 1996; Rostami et al., 2016; Shen et al., 2015). Despite the increased use of HER2-targeted therapies for the treatment of primary tumors and extracranial disease, HER2-targeted therapies have not been successful in the context of brain metastases in part due to poor blood-brain barrier (BBB) penetrance and emergence of resistance to HER2-targeted therapies (Lin et al., 2004, 2013; Pestalozzi and Brignoli, 2000; Stemmler et al., 2007). Because the brain serves as a unique sanctuary for HER2+ residual disease, brain metastases are increasingly observed in patients with HER2+ breast cancer, threatening to

counteract the progress made in patient survival by HER2-targeted therapies (Aversa et al., 2014).

Interestingly, it has been reported that approximately 15%–20% of patients with HER2– primary tumors become HER2+ upon colonization of the brain, suggesting a causal link between expression of this oncogene and the outgrowth of brain metastases (Hulsbergen et al., 2020; Priedigkeit et al., 2017). In triple-negative breast cancer mouse models, HER2 expression has been shown to promote breast cancer metastatic outgrowth in the brain (Palmieri et al., 2007). In patient samples, *ERBB2* mRNA was increased up to 5-fold in the brain metastases compared with HER2+ primary tumors (Palmieri et al., 2007). HER2 expression and activity is upregulated in solid tumors through multiple mechanisms including gene amplification, enhanced transcription, and genetic mutations (Andrulis et al., 1998; Kraus et al., 1987; Petrelli et al., 2017). However, the contribution of these and other mechanisms to the acquisition of brain metastatic competence remains to be defined.

The Abelson (ABL) family, ABL1 and ABL2, are non-receptor tyrosine kinases that potentiate signaling downstream of a diverse range of cellular stimuli, including cell-surface receptors such as epidermal growth factor receptor (EGFR) and HER2 (Plattner et al., 1999; Srinivasan et al., 2009; Wang and Pendergast, 2015). HER2 was reported to bind to ABL kinases, leading to their activation (Kurmi et al., 2018; Srinivasan et al., 2009). Conversely, ABL kinases have been shown to regulate the stability of the HER2 family member EGFR by decreasing EGFR endocytosis and subsequent degradation (Tanos and Pendergast, 2006). Recently, ABL kinases have been shown to play critical roles in solid tumor metastasis (Gu et al., 2016; Hoj et al., 2019; Wang et al., 2016). Inhibition of the ABL kinases impairs breast cancer metastasis to the bone and lung adenocarcinoma metastasis to the brain by regulating transcriptional networks (Hoj et al., 2019; Wang et al., 2016). These studies implicate ABL kinases in metastasis and highlight the potential clinical utility of targeting this signaling axis.

Here, we report that ABL kinase inhibitors impair translation of *ERBB2* by disrupting binding of the RNA-binding protein Y-box-binding protein 1 (YB-1) to *ERBB2* mRNAs. YB-1 activity has been implicated in a wide variety of cancers and has been shown to mediate tumor cell proliferation, invasion, metastasis, and drug resistance (Johnson et al., 2019). It has been suggested that YB-1 functions to disrupt the secondary structure of 5′ UTR stem loops and increase the translational efficiency of some mRNAs (Evdokimova et al., 2009). We found that loss of YB-1 expression in HER2+ breast cancer brain metastatic cells decreases HER2 protein levels and dramatically reduces cell viability *in vitro*. Notably, we show that knockdown of YB-1 significantly impairs brain metastatic outgrowth and improves mouse survival. We found that increased ABL kinase activity enhances tyrosine phosphorylation of YB-1 and that ABL-mediated YB-1 phosphorylation is required for HER2 translation. Our findings reveal a mechanism for translational regulation of HER2 and identify an ABL-YB-1 signaling axis targeting not only HER2 but also other cell-surface receptors implicated in brain metastasis. The discovery that cancer cells expressing HER2 can be targeted by BBB-permeable ABL kinase allosteric inhibitors suggests that these drugs might be effective to treat brain metastases driven by HER2 in breast cancer and other solid tumors.

RESULTS

ABL inhibition impairs tumor outgrowth in the brain and improves overall survival of mice with HER2+ breast cancer brain tumors

Due to the increasing prevalence of brain metastases in patients who are HER2+, the unmet clinical need for new therapies, and the reported HER2-induced ABL kinase activation, we evaluated the consequences of ABL kinase inhibition on brain colonization using a panel of brain metastatic HER2+ breast cancer cells. Human HER2+ brain metastatic HCC1954-LCC1 cells (Malladi et al., 2016) labeled with luciferase-GFP were injected intracranially into athymic nude mice. Mice bearing intracranial tumors were treated with vehicle or the ABL kinase allosteric inhibitor GNF5 (Figure 1A). An ABL allosteric inhibitor ABL001 is FDA-approved for BCR-ABL+ leukemia and has been shown to have blood-tumor-barrier penetrance *in vivo* (Hoj et al., 2019; Wylie et al., 2017). Strikingly, treatment with GNF5 decreased colonization of the brain parenchyma and increased overall survival in mice compared with vehicle (Figures 1B and 1C). Analysis of HCC1954-LCC1 brain tumor cell lysates showed that ABL kinase activity was decreased ~80% in the GNF5-treated mice as indicated by decreased phosphorylation of the ABL substrate CrkL (Figure S1A).

In vitro treatment with GNF5 and ABL001 markedly impaired cell viability in the HER2+ brain metastatic lines HCC1954-LCC1 and SUM190-BrM (Figures 1D and 1E) (Gril et al., 2018). Next, ABL kinases were genetically depleted in HCC1954-LCC1 cells using CRISPR-Cas9 (Figures 1F and S1E). CRISPR knockout of ABL1 and ABL2 reduced cell viability (Figures 1G and S1F). Further, CRISPR knockout of ABL1 and ABL2 in HCC1954-LCC1 cells decreased brain tumor burden and significantly improved overall survival following intracranial injection (Figures 1H–1J). These data support a role for ABL kinases in promoting outgrowth of HER2+ breast cancer brain metastatic cells.

To evaluate whether ABL kinases promote brain metastatic outgrowth in an immunocompetent mouse model, we employed the mouse HER2+ breast cancer brain metastatic cell line ErbB2-BrM2, derived from the MMTV-NeuNT mouse model (Muller et al., 1988; Valiente et al., 2014). ErbB2-BrM2 cells were injected intracranially into FVB mice, and mice were treated with vehicle or ABL001 (Figure 1K). Brain metastatic outgrowth was significantly impaired in mice treated with ABL001 compared with vehicle (Figures 1L–1M). Further, pharmacologic inhibition and genetic depletion of ABL kinase activity decreased ErbB2-BrM2 colony formation *in vitro* (Figures S1B–D). Together, these data demonstrate that ABL kinase allosteric inhibition impairs metastatic outgrowth and enhances survival of mice bearing brain metastatic HER2+ breast cancer cells.

ABL kinases regulate HER2 protein levels in HER2+ breast cancer brain metastatic cells

Unexpectedly, inhibition of ABL kinases with GNF5 or ABL001 dramatically decreased total HER2 protein levels, as detected by western blotting, in HCC1954-LCC1, ErbB2-BrM2, and SUM190-BrM cells (Figures 2A, 2C, and S2C). Conversely, treatment with the ABL kinase allosteric activator DPH more than doubled HER2 protein levels in HCC1954-LCC1 cells (Figure 2A) (Yang et al., 2011). To demonstrate that the effects of GNF5 and ABL001 on HER2 were on target, ABL kinases were depleted genetically using lentiviral

short hairpin RNAs (shRNAs). HCC1954-LCC1 cells were virally transduced with shRNAs targeting a scramble control (shScr) or both ABL1 and ABL2 (shAA). HER2 protein levels decreased ~60% in the shAA cells compared with the shScr control (Figure 2B). Immunofluorescence staining of HCC1954-LCC1 tumors following treatment with vehicle or GNF5 revealed decreased HER2 protein in the GNF5-treated mice (Figures S2A and S2B). Because HER2 signaling occurs predominantly at the plasma membrane, HER2 cell surface levels were quantified in DMSO or GNF5-treated ErbB2-BrM2 and SUM190-BrM cells by fluorescence-activated cell sorting (FACS) analysis. The cell surface expression of HER2 was reduced upon treatment with GNF5 in both ErbB2-BrM2 and SUM190-BrM cells (Figures 2D and S2D). The changes in HER2 protein were observed even when cell viability and apoptosis were not significantly altered, implying that loss of HER2 is not solely due to reduced cell viability (Figures S2E–S2H). These findings suggest that ABL kinases regulate HER2 protein levels in HER2+ brain metastatic breast cancer cells.

ABL kinases promote translation of HER2 in breast cancer brain metastatic cells

To investigate the mechanisms whereby ABL kinases regulate HER2 protein levels, we tested whether ABL kinase inhibition altered *ERBB2* transcription, protein stability, and/or translation. Pharmacologic and genetic inhibition of ABL kinases resulted in little to no change in *ERBB2* mRNA levels, suggesting that transcriptional regulation of *ERBB2* is unlikely to be the principal contributor for the profound decrease in HER2 protein expression (Figures 3A–3C). Further, we found that ABL kinase inhibition profoundly decreases HER2 protein levels in the ErbB2-BrM2 cells (Figures 2C and 2D), which expresses HER2 under the MMTV promoter instead of the endogenous HER2 promoter (Muller et al., 1988; Valiente et al., 2014). Conversely, ABL activation with DPH slightly increased *ERBB2* mRNA levels (Figure S3A) but did not fully account for changes observed at the protein level (Figure 2A). Thus, these data support the conclusion that ABL kinases do not affect HER2 transcription.

We next examined whether ABL kinases regulate HER2 protein stability. The half-life of HER2 was not significantly changed in GNF5-treated cells compared with control in the presence of the translation inhibitor cycloheximide (Figures S3B and S3C). Upon dissociation from the Hsp90 chaperone, HER2 can be degraded through the ubiquitin-proteasomal pathway (Mimnaugh et al., 1996). To assess whether ABL kinase inhibition promotes HER2 proteasomal degradation, GNF5-treated cells were cultured in the presence of the proteasomal inhibitor MG132. MG132 did not rescue HER2 protein levels in HCC1954-LCC1 and ErbB2-BrM2 cells treated with GNF5 (Figures 3D and 3E). Together, these data suggest that ABL kinases do not regulate HER2 protein stability through the ubiquitin-dependent proteasome pathway.

To determine the effects of ABL kinase inhibition on *ERBB2* translation, polysome fractionation was first employed. Canonically, mRNAs that associate with polyribosomes (heavy fractions) are considered translationally active, while mRNAs enriched in the messenger ribonucleoprotein (mRNP) fractions are considered "free" or non-translated targets. While no changes were observed in control β-actin (*ACTB*) mRNA polysome association, *ERBB2* mRNA association with heavy polyribosomes was marginally decreased

in GNF5-treated cells compared with DMSO-treated cells (Figures S3E and S3F). Treatment of ErbB2-BrM2 cells with the ABL kinase activator DPH did not alter *ERBB2* mRNA polyribosome association (Figures S3G–S3I).

Polysome fractionation provides a measure of ribosomal occupancy on mRNA, but it does not assess translational activity state. To directly assay the effect of ABL kinase inhibition on *ERBB2* mRNA translation, DMSO- and GNF5-treated HCC1954-LCC1 and ErbB2-BrM2 cells were pulsed with [^{35}S]methionine/cysteine (Met/Cys) to label nascent proteins, and following radiolabeling, immunoprecipitation (IP) of HER2 was performed. We found that [^{35}S]Met/Cys incorporation into the HER2 protein was significantly lower in cells treated with GNF5 (Figures 3F–3I). Similarly, genetic inhibition of ABL kinases in HCC1954-LCC1 cells led to a profound reduction in radiolabeled HER2 protein compared with the scramble control (Figures 3J and 3K). Conversely, treatment with DPH significantly increased [^{35}S]Met/Cys incorporation into HER2 protein (Figures 3L–3M). These data, in combination with the polysome profiling, suggest that ABL kinases may regulate translation elongation rather than translation initiation. To measure global translation changes, total protein incorporation of [^{35}S]Met/Cys was assessed. GNF5 decreased global translation whereas genetic inhibition of the ABL kinases only slightly reduced global translation (Figures S3J–S3M). Additionally, DPH treatment decreased global translation, opposite of the changes observed in *ERBB2* mRNA translation (Figures S3L and S3M). Together, these data show that ABL kinase inhibition or ABL knockdown impairs *ERBB2* mRNA translation, which leads to a decrease in HER2 protein levels in brain metastatic cells. However, these changes are not likely due to a decrease in global translation.

ABL kinase inhibition does not affect RISC-mediated silencing of HER2

There are several mechanisms by which ABL kinases could regulate *ERBB2* mRNA translation. ABL kinases could (1) affect *ERBB2* mRNA stability, (2) regulate microRNAs (miRNAs) targeting *ERBB2*, and/or (3) target a subset of RNA-binding proteins that interact with *ERBB2* to modulate its translation. First, *ERBB2* mRNA stability was measured in ErbB2-BrM2 and HCC1954-LCC1 cells by treating with DMSO or GNF5 and the transcription inhibitor actinomycin-D. *ERBB2* mRNA stability was not significantly altered in ErbB2-BrM2 cells but was slightly increased in GNF5-treated HCC1954-LCC1 cells (Figures S4A and S4B). These data suggest that decreased *ERBB2* mRNA translation upon ABL inhibition is not likely due to lower *ERBB2* mRNA stability.

Multiple miRNAs have been reported to target *ERBB2* (Leivonen et al., 2014). Thus, we evaluated whether ABL inhibition impaired HER2 protein levels in cells depleted of the RNA-induced silencing complex RISC, which mediates miRNA gene silencing. ErbB2-BrM2 and HCC1954-LCC1 cells were transduced with lentiviruses expressing shRNAs targeting the core Argonaute proteins of the RISC complex (AGO1, AGO2, AGO3, and AGO4) (shAGO1–4) or a non-target control (shNTC) (Figures S4C and S4E), and these cells were then treated with DMSO or GNF5. Knockdown of the Argonaute proteins did not rescue HER2 protein levels in ABL inhibited cells (Figures S4D and S4F). While these data support the hypothesis that ABL kinases do not target miRNA-mediated silencing through

the RISC complex to regulate HER2 translation, these findings do not entirely eliminate a role for miRNAs in this process.

ABL kinase inhibition disrupts the interaction of RNA-binding protein with *ERBB2* mRNA

RNA-binding proteins play a critical role in mRNA processing, transport, stability, and translation. To examine whether ABL kinase inhibition affects *ERBB2* mRNA-binding proteins, the *ERBB2* 5′ UTR, 3′ UTR, and coding sequence (CDS) mRNAs were biotinylated, bound to streptavidin magnetic beads, and incubated with lysates from DMSO- or GNF5-treated HCC1954-LCC1 cells (Figure 4A). *ERBB2* mRNA-binding proteins were eluted and separated by gel electrophoresis, and bands corresponding to altered proteins between DMSO- and GNF5-treated samples were excised from the silver-stained gel and identified by mass spectrometry (Figures 4B and S4G; Table S1). Immunoblot analysis revealed that ABL kinase inhibition induced a profound decrease in association of two RNA-binding proteins with the *ERBB2* CDS: YB-1 and Lupus La protein (SSB) (Figure 4C). Notably, RNA IP (RIP) of YB-1 followed by qRT-PCR revealed a reduced interaction between YB-1 and *ERBB2* mRNA upon ABL kinase inhibition in HCC1954-LCC1 and SUM190-BrM cells (Figures 4D and 4E). To confirm YB-1 binding of the *ERBB2* mRNA, previously generated YB-1 cross-linking IP (CLIP)-sequencing data of long RNA species (GEO: GSE63604) from breast cancer cells were analyzed (Goodarzi et al., 2015). Multiple YB-1 binding sites were identified within the *ERBB2* mRNA transcript (Figure 4F). Together, these data suggest that YB-1 binds to the *ERBB2* mRNA and loss of ABL kinase activity disrupts this interaction.

Loss of YB-1 decreases HER2 protein levels and ablates metastatic outgrowth in the brain

To determine whether YB-1 depletion regulates HER2 protein levels, YB-1 expression was reduced using multiple shRNAs. YB-1 knockdown in HCC1954-LCC1 and SUM190-BrM cells markedly decreased HER2 protein levels without reducing global protein expression or expression of selected proteins such as SOX2 and MMP9 (Figures 5A and S5A–S5C). Importantly, overexpression of YB-1 rescued HER2 protein levels in GNF5-treated HCC1954-LCC1 cells (Figure 5B). Loss of YB-1 did not affect *ERBB2* transcription (Figure S5D). Further, YB-1 predominately localizes to the cytoplasm, and its localization is not significantly affected by ABL kinase inhibition in HCC1954-LCC1 cells (Figures S5G and S5H). Because knockdown of SSB marginally decreased HER2 protein levels in HCC1954-LCC1 cells, but not in SUM190-BrM cells (Figures S5E and S5F), we focused on YB-1 due to the conserved effects of YB-1 loss on HER2 expression across multiple HER2+ brain metastatic cell lines. To directly assess whether YB-1 affects HER2 translation, HCC1954-LCC1 cells were virally transduced with YB-1 shRNAs. Cells were pulsed with [^{35}S]Met/Cys, and radiolabeled HER2 protein was immunoprecipitated and quantified (Figures 5C, 5D, and S5I). Loss of YB-1 decreased the amount of newly synthesized HER2 protein. These data support a role for YB-1 in regulating HER2 translation.

Next, we evaluated whether loss of YB-1 affected HER2+ breast cancer cell viability. HCC1954-LCC1 and SUM190-BrM cells transduced with shRNAs targeting YB-1 (shYB-1) had markedly reduced cell viability *in vitro* compared with non-target control (shNTC) cells (Figures 5E, S5J, and S5K). The marked decrease in cell viability elicited

by YB-1 loss was comparable to the profound decrease in cell viability induced by HER2 knockdown (Figures 5F and S5L). Overexpression of HER2 in YB-1-depleted cells rescued cell viability, suggesting that the loss of HER2 contributes to the loss in cell viability (Figure 5G). To evaluate the effect of YB-1 knockdown on brain metastatic outgrowth *in vivo*, athymic nude mice were injected intracranially with HCC1954-LCC1 or SUM190-BrM cells expressing shNTC or shYB-1 shRNAs. Loss of YB-1 reduced brain tumor burden (Figures 5H, 5I, S5M, S5N, S5P, and S5Q). Further, mice bearing HCC1954-LCC1 shYB-1 tumors had markedly improved overall survival compared with mice with shNTC tumors (Figures 5J and S5O). Notably, high expression of *YBX1* correlates with decreased distant metastasis free survival in patients with breast cancer (Figure 5K). Mutual exclusivity analysis revealed that *ABL1*, *ABL2*, *ERBB2*, and *YBX1* co-occur in human patients with breast cancer (Figure S5R). Together, these data show that YB-1 promotes HER2+ brain metastatic outgrowth and that loss of YB-1 impairs brain tumor burden and improves overall survival of mice. Since YB-1 has previously been shown to have many pro-oncogenic and pro-survival functions, we cannot rule out that these other mechanisms may underlie some of the observed phenotypes (Bargou et al., 1997; Evdokimova et al., 2009; Jiang et al., 2022; Lim et al., 2017; Shah et al., 2020).

ABL kinases phosphorylate YB-1, and tyrosine phosphorylated YB-1 is required for *ERBB2* translation and HER2 protein expression

Next, we sought to identify how ABL kinases regulate YB-1. Since ABL kinases function as tyrosine kinases, we assessed tyrosine phosphorylation of YB-1 in the presence of a hyperactive form of ABL1 (ABL1PP). HEK-293T cells were co-transfected with a GFP-tagged YB-1 (EGFP-YB-1) or a 3×FLAG-tagged YB-1 (3×FLAG-YB-1) and ABL1PP. ABL1PP increased tyrosine phosphorylation of epitope-tagged YB-1 (Figures 6A and S6A). EGFP-YB-1 was also tyrosine phosphorylated in the presence of a hyperactive form of ABL2 (ABL2PP) but to a lesser degree than that observed in cells expressing ABL1PP (Figure S6B). HEK-293T cells co-transfected with EGFP-YB-1 and ABL1PP were treated with DMSO or GNF5 (Figure 6B). GNF5 decreased the tyrosine phosphorylation of eGFP-YB-1. These data show that ABL kinase activity promotes tyrosine phosphorylation of YB-1 and that ABL-specific allosteric inhibitors decrease tyrosine phosphorylated YB-1.

To determine whether ABL kinases associate in the same complex as YB-1, HEK-293T cells were co-transfected with EGFP-YB-1 and ABL1PP or ABL2PP. Following EGFP-YB-1 IP with anti-GFP antibody, immunoblotting revealed coIP with ABL1PP and ABL2PP (Figures 6C and S6C). Further, reciprocal coIP of EGFP-ABL1PP showed an association of EGFP-ABL1PP with 3×FLAG-tagged YB-1 (Figure 6D). Next, we assessed whether activated ABL kinases could promote tyrosine phosphorylation of YB-1 in the human HER2+ brain metastatic cell lines. Transfection of HCC1954-LCC1 cells with ABL1PP markedly increased tyrosine phosphorylation of EGFP-YB-1 (Figure 6E). Further, in SUM190-BrM cells, treatment with ABL001 reduced tyrosine phosphorylation of EGFP-YB-1 (Figure 6F). These data show ABL-dependent tyrosine phosphorylation of YB-1 in HER2+ breast cancer cells. To assess whether ABL1 directly phosphorylates YB-1, we performed an *in vitro* kinase assay using purified GST-tagged ABL1 and His-tagged YB-1 proteins.

ABL1 increased tyrosine phosphorylation of YB-1 *in vitro* (Figure 6G). Together, these data suggest that ABL kinases form a complex with YB-1 and phosphorylate YB-1.

To identify which YB-1 domain is necessary for its interaction with ABL1, the three main YB-1 domains (Figure 6H) were used: (1) the alanine/proline (A/P)-rich domain, (2) the cold-shock domain (CSD), and (3) the C-terminal domain (Wolffe, 1994; Wolffe et al., 1992). The CSD binds to DNA and RNA, and the C-terminal domain regulates protein-protein interactions. We found that ABL1PP interacts most strongly with the CSD and weakly with the C-terminal domain (Figure 6I). To evaluate whether RNA is essential for this interaction to occur, lysates were treated with RNase before coIP. Interestingly, RNase treatment increased the interaction between ABL1 and YB-1 domains (Figure S6D). These data suggest the ABL1-YB-1 interaction does not occur through RNA binding.

To determine which domain of YB-1 is tyrosine phosphorylated downstream of ABL1PP, we co-transfected HEK-293T cells with ABL1PP and the GFP-tagged YB-1 domains containing tyrosine residues. Both the CSD and the C-terminal domain had increased tyrosine phosphorylation, suggesting that increased ABL1 activity leads to phosphorylation of multiple tyrosine residues (Figure 6J). Since there are only two tyrosine residues in the CSD of YB-1, these residues (Y72 and Y99) were mutated individually to phenylalanine (Y72F and Y99F). ABL-dependent tyrosine phosphorylation was reduced upon Y72F and Y99F mutations (Figure S6E). These data suggest that ABL activity leads to phosphorylation of both tyrosine residues.

To determine the functionality of phosphorylation at Y72 and Y99, both residues were mutated to phenylalanine in GFP-tagged YB-1 (GFP-YB-1 Y72/99F). Notably, we found that in HCC1954-LCC1 breast cancer cells transduced with shYB-1 #1, expression of GFP-tagged YB-1 wild type partially rescues HER2 protein levels (Figure 6K). The partial rescue might be due to the large GFP tag on YB-1, which could interfere with its translational activity. Importantly, expression of the phospho-deficient GFP-YB-1 Y72/99F mutant profoundly decreases HER2 protein levels in these breast cancer cells (Figure 6K). This decrease might be explained by previous work showing that homodimerization of the CSD is critical for the YB-1-RNA interaction, which is mediated through Y72 and Y99 (Yang et al., 2019). Similarly, HER2 translation as measured by [^{35}S]-Met/Cys was rescued in YB-1-depleted cells upon expression of GFP-tagged YB-1 wild type but not in cells expressing GFP-YB-1 Y72/99F (Figure 6L). Thus, these data show that tyrosine phosphorylation of the YB-1 CSD regulates HER2 protein translation.

ABL kinases regulate YB-1 binding to mRNAs encoding brain metastatic targets

Over 50 transcripts related to breast cancer metastasis were evaluated for YB-1 binding sites using the YB-1 CLIP-sequencing (CLIP-seq) dataset (GEO: GSE63604) (Goodarzi et al., 2015) (Tables S2 and S3). In addition to *ERBB2*, *AXL*, *L1CAM*, S*REBF1*, *HMG20B*, and *RPL13* were identified as YB-1 binding targets, and a subset of these mRNAs were shown to have decreased YB-1 binding to their mRNA upon GNF5 treatment (Figures S7A and S7B). Consistent with a functional ABL-YB-1 signaling axis, we found that knockdown of YB-1 or GNF5 treatment markedly decreases AXL and L1CAM protein levels in HCC1954-LCC1 breast cancer cells (Figures S7C, S7E, S7J, and S7L). Importantly, depletion of YB-1 did

not affect *AXL* and *L1CAM* mRNA expression (Figures S7D and S7K). Thus, these data support a role for ABL-dependent translational regulation of a subset of transcripts through YB-1 in breast cancer brain metastatic cells.

To determine whether the decrease in AXL and L1CAM contribute to the loss of cell viability upon YB-1 knockdown in breast cancer cells, HCC1954-LCC1 cells were transduced with shRNAs targeting AXL or L1CAM, and cell viability was measured. AXL knockdown reduced cell viability compared with a non-target control (shNTC) (Figures S7F–S7I). In contrast, L1CAM knockdown did not significantly affect cell viability in the breast cancer cells (Figures S7M and S7N). These data suggest that decreased AXL, but not L1CAM, protein levels may contribute in part to decreased cell viability upon YB-1 knockdown.

ABL kinase inhibition decreases mutant HER2 protein levels in lung cancer cells

Approximately 47% of patients with mutant HER2-driven lung cancer will develop brain metastases (Offin et al., 2019). Currently, there are no HER2-targeted therapies for HER2-mutant lung cancer (Zhao and Xia, 2020). We hypothesized that ABL kinase inhibition might also deplete mutant HER2 protein levels. To test this hypothesis, the human HER2-mutant lung cancer line NCI-H1781 was treated with DMSO or ABL001. ABL001 profoundly decreased mutant HER2 protein levels (Figure 7A) and markedly reduced cell viability *in vitro* (Figure 7B). Further, RIP of YB-1 from NCI-H1781 cells treated with ABL kinase inhibitor revealed that ABL001 treatment disrupted YB-1 binding to mutant *HER2* mRNA (Figure 7C). Moreover, YB-1 knockdown decreased mutant HER2 protein levels and reduced NCI-H1781 cell viability (Figures 7D and 7E). These data support a role for an ABL-YB-1 axis in the regulation of mutant HER2.

DISCUSSION

While mechanistic studies have examined the regulation of HER2 overexpression in tumors via gene amplification and transcriptional changes, the mechanisms that drive HER2 translation, particularly in the context of brain metastasis, are relatively unknown. Here, we report an ABL-YB-1 signaling axis that regulates a translational program targeting *ERBB2* and other transcripts implicated in brain metastasis. We show that ABL kinase inhibition decreases translation of HER2 and disrupts YB-1 binding to the *ERBB2* mRNA CDS in breast cancer brain metastatic cells (Figure 7F). YB-1 functions primarily as an RNA-binding protein but can also translocate to the nucleus, where it serves as a transcription factor. Previous studies have shown that YB-1 is elevated in most human breast cancers and can modulate drug resistance by increasing transcription of a multidrug transporter (Bargou et al., 1997). Our data revealed that YB-1 has a critical role in binding to a subset of mRNAs including *ERBB2* in brain metastatic breast cancer cells. We found that YB-1 localizes primarily to the cytosol and that knockdown of YB-1 does not affect *ERRB2* mRNA levels. These data suggest that YB-1 promotes HER2 translation in breast cancer brain metastases without altering *ERBB2* transcription.

RNA-binding proteins play a role in mRNA-specific translational control, and previous studies have found that YB-1 can disrupt the highly structured 5′ UTR of *HIF1A* and

SNAI1, allowing binding by the eIF4E translation initiation complex (El-Naggar et al., 2015; Evdokimova et al., 2009). While many studies have focused on binding to the 5′ and –3′ UTR of mRNA transcripts, emerging evidence suggests that proteins can bind within the coding region to affect translation. For example, members of the DEAD-box family of RNA helicases bind to the coding region of mRNAs and remodel the secondary structure to enhance translation (Jungfleisch et al., 2017). Interestingly, acute translation, but not polysome profiling, was altered by ABL kinase inhibition. These data support a role for ABL kinases in translation elongation rather than translation initiation. YB-1 may promote mRNA translation elongation of *ERBB2* by disrupting its secondary structure.

In breast cancer, mRNA-specific translational control of metastatic targets can be enhanced through deregulation of ribosomal proteins and RNA-binding proteins. Overexpression of the ribosomal subunit RPL15 increased breast cancer metastatic burden by selectively promoting the translation of mRNAs encoding proteins required for cell proliferation (Ebright et al., 2020). The N6-methyladenosine reader YTHDF3 is upregulated in brain metastases and enhances translation of a subset of mRNAs including S*T6GALNAC5*, *GJA1*, and *EGFR*, all of which promote extravasation and colonization of the brain parenchyma (Chang et al., 2020). Our data show that loss of YB-1 impairs metastatic outgrowth in the brain by targeting the *ERBB2* mRNA.

In addition to *ERBB2*, YB-1 also binds to *AXL* and *L1CAM* mRNAs, which encode cell-surface receptors that have been implicated in brain metastasis (Hoj et al., 2019; Valiente et al., 2014). Interestingly, AXL has also been shown to promote resistance to HER2-targeted therapies, and its dimerization with HER2 leads to enhanced metastatic potential in HER2+ breast cancer (Goyette et al., 2018; Liu et al., 2009). Inhibition of the ABL-YB-1 signaling axis markedly decreases HER2, L1CAM, and AXL protein levels without affecting the expression of the corresponding mRNAs. While knockdown of HER2 and, to a lesser extent, AXL decreased breast cancer cell viability, knockdown of L1CAM did not. Thus, our data suggest that loss of cell viability upon YB-1 knockdown is mediated primarily through HER2 and, to a lesser extent, through AXL.

HER2 mutant lung cancer has a high propensity to metastasize to the brain (Offin et al., 2019). Currently, there are no approved targeted therapies for patients with mutant HER2-driven lung cancer (Zhao and Xia, 2020). The majority of HER2 mutations in non-small cell lung cancer occur in exon 20, which can confer resistance to HER2-targeted therapies (Baraibar et al., 2020). Since ABL kinases regulate the translation of HER2, we tested whether ABL kinase inhibition could affect mutant HER2 protein levels. The ABL kinase allosteric inhibitor ABL001, which is FDA approved for BCR-ABL1+ leukemia, ablated HER2 protein levels in the human mutant HER2-driven lung cancer line NCI-H1781, leading to reduced cell viability (Mauro et al., 2019). ABL kinase inhibition disrupted the binding of YB-1 to mutant HER2 mRNA, and loss of YB-1 decreased mutant HER2 protein. These data suggest that ABL kinases may also regulate mutant HER2 expression in BCBM and that ABL kinases may be an actionable target in mutant HER2+ tumors.

Our data show that binding of YB-1 to mRNAs of several cell-surface receptor proteins was markedly impaired by ABL kinase inhibition. Notably, we found that ABL kinases

phosphorylate YB-1 and that increased ABL kinase activity leads to phosphorylation of YB-1 in both the CSD and the C-terminal domains. Interestingly, previous work has identified a role for tyrosine residues Y72 and Y99 in the recognition of RNA-binding sequence motifs and homodimerization of YB-1 (Yang et al., 2019). Here, we show that while YB-1 wild type rescues HER2 translation and protein expression in YB-1-depleted breast cancer cells, the YB-1 Y72/Y99F phospho-deficient mutant fails to rescue HER2 translation and protein levels in these cells. Together, these data support the hypothesis that tyrosine phosphorylation at Y72 and Y99 of YB-1 impacts its ability to recognize and bind *ERBB2* mRNA. Our data revealed that loss of ABL-mediated YB-1 tyrosine phosphorylation disrupts its binding to *ERBB2* mRNA. These findings support the use of ABL kinase allosteric inhibitors for the treatment of HER2+ brain metastasis and suggest that these inhibitors may be used to target YB-1 translational activity by disrupting the binding to *ERBB2* and a subset of other transcripts encoding for proteins implicated in brain metastasis.

Limitations of the study

While we were able to assess the effects of inhibition of YB-1 tyrosine phosphorylation at Y72 and Y99 using phospho-deficient mutations, we did not perform rescue studies with phospho-mimetic mutants. Phenylalanine and tyrosine residues are nearly identical except for the hydroxyl group on the tyrosine residue, which serves as the site of phosphorylation. However, phospho-mimetic mutations of tyrosine residues to glutamate do not accurately recapitulate the spatial and ionic binding presented by phosphotyrosine residues and, consequently, often fail to elicit proper structure-function regulation. To evaluate the role of ABL kinases in the regulation of mutant HER2 in tumor types other than breast cancer, we employed the NCI-H1781 lung cancer cell line. Future studies should employ additional HER2-mutant cell lines as well as primary tumor cells expressing mutant HER2 to assess sensitivity to ABL kinase allosteric inhibitors.

STAR★METHODS

RESOURCE AVAILABILITY

Lead contact—Further information and requests for resources and reagents should be directed to, and will be fulfilled by, the corresponding author and Lead Contact, Ann Marie Pendergast (ann.pendergast@duke.edu).

Materials availability—All unique and stable reagents generated in this study are available from the Lead contact upon completion of a Materials Transfer Agreement.

Data and code availability

- The mass spectrometry dataset generated during this study has been deposited in the University of California, San Diego Mass Spectrometry Interactive Virtual Environment (MassIVE) under identifier: MSV000087674. Immunoblot data have been deposited at Mendeley Data and are publicly available as of the date of publication. DOIs are listed in the key resources table. This paper analyzes

existing publicly available data. These accession numbers for the datasets are listed in the key resources table.

- This paper does not report original code.

- Any additional information required to reanalyze the data reported in this paper is available from the lead contact upon request.

EXPERIMENTAL MODEL AND SUBJECT DETAILS

Animal models—All procedures involving mice were approved and performed following the guidelines of the IACUC of Duke University Division of Laboratory Animal Resources. For studies using human breast cancer cells, we employed 8–12-week old age-matched female outbred athymic nu/nu mice (#007850; RRID: IMSR_JAX:007850) purchased from The Jackson Laboratory. For immunocompetent studies, 8–12-week old age-matched female FVB/NJ mice (Jackson Laboratory; #001800; RRID: IMSR_JAX:001800) were injected intracranially with murine-derived ErbB2-BrM2 cells. The mice were maintained under pathogen-free conditions in the Duke Cancer Center Isolation Facility for immune-deficient mice.

Cell lines and cell culture—HCC1954-LCC1 and ErbB2-BrM2 cells were a gift from Dr. Joan Massagué (Memorial Sloan Kettering Cancer Center, New York, NY, USA). SUM190-BrM cells were a gift from Dr. Patricia Steeg (National Cancer Institute, Bethesda, MD, USA). HCC1954-LCC1, ErbB2-BrM2, and SUM190-BrM cells were originally isolated from female breast cancer patients. HEK293T (female) and NCI-H1781 (female) cells were purchased from the Duke University Cell Culture Facility. HCC1954-LCC1 cells were maintained in RPMI 1640 (Life Technologies) supplemented with 10% fetal bovine serum (FBS, Corning) and 1% antibiotic-antimycotic (Life Technologies). ErbB2-BrM2 and HEK293T cells were maintained in DMEM (Life Technologies) supplemented with 10% FBS (Corning) and 1% penicillin-streptomycin (Life Technologies). SUM190-BrM cells were maintained in F12 (Life Technologies) supplemented with 1× insulin-transferrin-selenium-ethanolamine (Life Technologies), 1 ug/mL hydrocortisone (Sigma), 10 mM HEPES (Life Technologies), 10 nM tri-iodo thyronine (T3) (Sigma), and 1.0 g/L bovine serum albumin (Sigma). 2% FBS (Corning) was added to the media for SUM190-BrM cell adherence but was removed for every subsequent feeding. NCI-H1781 cells were maintained in RPMI 1640 (Life Technologies) supplemented with 10% FBS (Corning), 1 mM sodium pyruvate (Life Technologies), 10 mM HEPES (Life Technologies), and 0.2% glucose (Sigma). All cultures were maintained at 37°C in humidified air with 5% CO_2. For *in vitro* pharmacologic treatments with GNF5, ABL001, or DPH, drugs were dissolved in DMSO and replaced every 24 hours. GNF5 and ABL001 were synthesized by the Duke Small Molecule Synthesis Facility and verified by LC-MS, ^{1}H-NMR, and cell-based assays. DPH was purchased from Sigma-Aldrich and validated by cell-based assays.

METHOD DETAILS

DNA plasmids—Sequences for shRNAs targeting the ABL kinases were as follows: scrambled shRNA (GGTGTATGGGCTACTATAGAA); *ABL1* shRNA (GGTGTATGAGCTGCTAGAGAA); *ABL2* shRNA (CCTTATCTCACCCACTCTGAA).

Stable non-inducible shRNAs against non-target control (NTC), *AGO1*, *AGO2*, *AGO3*, *AGO4*, *YBX1*, *SSB*, *ERBB2*, *AXL*, and *L1CAM* were from the Sigma Mission TRC1 Lentiviral shRNA library and were obtained through the Duke Functional Genomics Shared Resource Facility. Sigma clone identifiers are listed in the key resources table. The lentiCas9-blast plasmid was a gift from Dr. Feng Zhang (Addgene #52962) (Sanjana et al., 2014). The perbB2-ECFP plasmid was a gift from Martin Offterdinger (Addgene #40268) (Offterdinger and Bastiaens, 2008). The TetO-FUW-pgk-puro was a gift from Emily Dykhuizen (Addgene plasmid # 85747; http://n2t.net/addgene:85747; RRID:Addgene_85747) (Chowdhury et al., 2016).

Cloning—For pLKO-shYB1 #2-puro, the shRNA sequence corresponding to *YBX1* (GGTTCCCACCTTACTACAT) (Shibata et al., 2013) was cloned into the pLKO.1-puro backbone. Briefly, sense and anti-sense oligos for respective shRNA sequences flanked by 5′ AgeI and 3′ EcoRI restriction site overhangs were mixed in 1× annealing buffer (100 mM NaCl, 10 mM Tris-HCl, pH 7.4) and annealed by placing in boiling water that was allowed to cool to 25°C. pLKO.1-shNTC-puro (Sigma Mission TRC1 Lentiviral shRNA library) was digested with AgeI-HF (NEB) and EcoRI-HF (NEB) followed by gel purification using the QIAquick Gel Extraction Kit (QIAGEN). Gel-purified vector and annealed oligos were ligated using the Quick Ligation kit (NEB) and subsequently transformed in One Shot Stbl3 chemically competent cells (Thermo Fisher). For the FUW-HER2-pgk-puro construct, HER2 was PCR amplified from the perbB2-ECFP plasmid using primers flanked with a 5′ and −3′ NheI restriction site (Forward: TAAGCAGCTAGCATGGAGCTGGCGGCCTTGTG; Reverse: TGCTTAGCTAGCTCACACTGGCACGTCCAGAC). The PCR product was gel purified. The PCR product and the TetO-FUW-pgk-puro were digested with NheI-HF (NEB) and the backbone was dephosphorylated using Quick CIP (NEB). The digested PCR product and backbone were gel-purified and annealed using T4 DNA ligase (NEB). The ligation product was transformed.

YB-1 construct cloning—The pDESTmycYBX1 was a gift from Dr. Thomas Tuschl (Addgene #19878) (Landthaler et al., 2008). The mEGFP-C1 backbone was a gift from Michael Davidson (Addgene #54759; http://n2t.net/addgene:54759; RRID:Addgene_54759). The N174-MCS backbone was a gift from Adam Karpf (Addgene #81061; http://n2t.net/addgene:81061; RRID:Addgene_81061). Full length and YB-1 domains were PCR amplified from pDESTmycYBX1 and flanked by a 5′ BspEI and 3′ BamHI restriction site. Sequences for PCR primers were as follows: 5′ BspEI YB-1 full length forward (TAAGCATCCGGAatgagcagcgaggccgagac), 3′ BamHI YB-1 full length reverse (TGCTTAGGATCCttactcagcccccgccctgct), 5′ BspEI YB-1 A/P domain forward (TAAGCAtccggaATGAGCAGCGAGGCCGAGACCC), 3′ BamHI YB-1 A/P domain reverse (TGCTTAggatccttaGTCCCCGCCGGCAGGCGC), 5′ BspEI YB-1 Cold shock domain forward (TAAGCAtccggaAAGAAGGTCATCGCAACGAA), 3′ BamHI YB-1 Cold shock domain reverse (TGCTTAggatccttaACCAGGACCTGTAACATTTG), 5′ BspEI YB-1 C-terminal domain forward (TAAGCAtccggaGGTGTTCCAGTTCAAGGCAG), and 3′ BamHI YB-1 C-terminal domain reverse (TGCTTAggatccTTACTCAGCCCCGCCCTG). The PCR products were gel purified. The PCR products were then cleaved with BspEI

(NEB) and BamHI-HF (NEB). The mEGFP-C1 backbone was cleaved with BspEI (NEB) and BamHI-HF (NEB) and dephosphorylated using Quick CIP (NEB). The cleaved PCR products and backbone were then gel purified. Gel purified backbone and PCR products were annealed using the Quick Ligation Kit (NEB). The ligation products were transformed. To clone the N174-eGFP-YB-1 vector, eGFP-YB-1 was PCR amplified from the mEGFP-YB-1-C1 (this paper) plasmid using primers flanked with a 5′ and –3′ NotI restriction site (Forward: TAAGCAgcggccgcATGGTGAGCAAGGGCGAGGA; Reverse: TGCTTAgcggccgcTTACTCAGCCCCGCCCTGCT). The PCR product was gel purified. The PCR product and N174-MCS backbone were cleaved with NotI-HF (NEB). The N174-MCS backbone was dephosphorylated using Quick CIP (NEB). The cleaved PCR product and backbone were gel purified. The PCR product and backbone were ligated using the Quick Ligation Kit (NEB). The ligation product was transformed. For TetO-FUW-eGFP-YB-1-pgk-puro and TetO-FUW-eGFP-YB-1 Y72/99F-pgk-puro, eGFP-YB-1 was PCR amplified from the mEGFP-YB-1-C1 plasmid using primers flanked with a 5′ and-3′ NheI restriction site (Forward: TAAGCAgc tagcATGGTGAGCAAGGGCGAGGA; Reverse: TGCTTAgctagcTTACTCAGCCCCGCCCTGCT). The PCR product was gel purified and cleaved with NheI-HF (NEB). TetO-FUW-pgk-puro was cleaved and dephosphorylated using Quick CIP (NEB). The PCR product and backbone were gel purified and ligated using the T4 DNA ligase (NEB). The ligation product was transformed. For the 3×FLAG-YB-1 plasmid, YB-1 was PCR amplified from pDESTmycYBX1 using primers flanked with a 5′ BamHI and 3′ XhoI restriction site (Forward: TAAGCAGGATCCatgagcagcgaggccgagac; Reverse: TAAGCACTCGAGttactcagccccgccctgct). The PCR product was gel purified and cleaved with BamHI-HF (NEB) and XhoI (NEB). The backbone 3×FLAG-FUS-WT was a gift from Robin Reed (Addgene #44985) (Yamazaki et al., 2012). The backbone was cleaved with BamHI-HF (NEB) and XhoI (NEB) and dephosphorylated with CIP (NEB). The cleaved PCR product and backbone were gel purified and ligated using T4 DNA ligase (NEB). The ligation product was transformed.

CRISPR-Cas9 cloning—The lentiGuide-Puro backbone was a gift from Dr. Feng Zhang (Addgene #52963) (Sanjana et al., 2014). The lentiGuide-Hygro (Addgene# 139462; http://n2t.net/addgene:139462; RRID:Addgene_139462) and lentiGuide-Neo backbones (Addgene #139449) were a gift from Dr. Caroline Goujon (Doyle et al., 2018). Oligonucleotides with mouse ABL1 gRNA (AAGGGAGGGTGTACCACTAC), mouse ABL2 gRNA (GCCCCGGAGCCTCCCCGACG), human ABL1 gRNA #1 (GGTTCATCATCATTCAACGG), human ABL1 gRNA #2 (CTTAGGCTATAATCACAATG), or human ABL2 gRNA #1 (GGTTCAACATCACAACCATA), or human ABL2 gRNA #2 (TATCGAATG GAACAGCCTGA) flanked by BsmBI 5′ or 3′ restriction site overhangs were phosphorylated and annealed using the T4 PNK (NEB). The lentiGuide backbones were cleaved and dephosphorylated using BsmBI (NEB) and CIP (NEB). The backbones were then gel purified using the QIAquick Gel Extraction Kit (QIAGEN). Gel purified backbone and annealed oligos were then ligated using the Quick Ligation Kit (NEB) (Sanjana et al., 2014). The ligation products were transformed in One Shot Stbl3 chemically competent cells (Thermo Fisher).

Mutagenesis—The GFP-ABL1PP plasmid was generated by site directed mutagenesis using the pcDNA-GFP-ABL1 plasmid (Burton et al., 2003). The mEGFP-YB1 CSD Y72F and mEGFP-YB1 CSD Y99F plasmid were generated using the mEGFP-YB1 CSD-c1 plasmid. The mEGFP-YB1 Y72/99F-c1 plasmid was generated using the mEGFP-YB1-c1 plasmid. PCR amplification was performed using the PfuUltra II Fusion High-fidelity DNA polymerase (Agilent) according to the manufacturer's instructions. The template DNA was digested using DpnI (NEB) and the remaining DNA was transformed into One Shot Stbl3 chemically competent cells (Thermo Fisher). Primers used for mutagenesis were as follows: ABL1 P249E Forward: tctcccacttgtcgtagttctcggacacaccatagacagtg; ABL1 P249E Reverse: cactgtctatggtgtgtccgagaactacgacaagtgggaga; ABL1 P242E Forward: ggacacaccatagacagtctccttgttgcgctttggggc; ABL1 P242E Reverse: gccccaaagcgcaacaaggagactgtctatggtgtgtcc; YB-1 Y72F Forward: cctgttgatgaaaccaaatccgttccttacattgaacc; YB-1 Y72F Reverse: ggttcaatgtaaggaacggatttggtttcatcaacagg; YB-1 Y99F Forward: acactgcgaaggaacttcctggggttattcttcttt; YB-1 Y99F Reverse: aaagaagaataaccccaggaagttccttcgcagtgt.

Lentiviral transduction—Lentiviral shRNAs and CRISPR-Cas9 constructs were packaged using 3rd generation lentiviral packaging plasmids (pMDL, RSV-Rev, and CMV-VSVG) as previously described (Chislock and Pendergast, 2013; Chislock et al., 2013; Smith-Pearson et al., 2010). For cells transduced with TetO-FUW-pgk-puro or TetO-FUW-HER2-pgk-puro, 2nd generation lentiviral packaging plasmids (pMD2.G, psPAX2). For TetO-FUW-pgk-puro or TetO-FUW-HER2-pgk-puro, cells were also transduced with pLVX-Tet-On Advanced (Clontech). Plasmid expression was induced using 1 μg/mL doxycycline (Sigma-Aldrich). HEK293T cells were transfected with the packaging and shRNA or CRISPR-Cas9 DNA using FuGENE 6 (Promega). After 48 hours, the viral titer was filtered using a 0.45 μm filter. For lentiviral transduction in the ErbB2-BrM2 cells, the viral titer was concentrated 10× using Lenti-X concentrator (Takara Bio) according to the manufacturer's instructions. The viral titer and 1.6 μL of 10 μg/mL polybrene (Sigma-Aldrich) was added to the target cells and the cells were centrifuged at 2250 RPM for 1 hour at 25°C. The viral titer was replaced with target cell maintenance media. When appropriate, cells were selected with puromycin at 1–2 μg/mL, blasticidin at 5–10 μg/mL, or hygromycin at 200–500 μg/mL.

Transient transfection—Transient transfections were performed using Lipofectamine 2000 (Invitrogen) according to the manufacturer's instructions. Cells were transfected with 2 μg of full length and truncated eGFP-YB-1 DNA or 3×FLAG-YB-1. Cells were transfected with 1.5 μg of pcDNA-ABL1PP, pcDNA-ABL2PP, or GFP-ABL1PP DNA for all experiments except for GNF5 drug treatment (Plattner et al., 2004). For GNF5 drug treatment, cells were transfected with 50 ng of Myc-His-ABL1PP. After 24 hours, cells were treated with DMSO or 40 μM GNF5 for 24 hours.

Immunoprecipitation—For YB-1 phosphorylation studies, cells were lysed in RIPA buffer (50 mM Tris HCl, 150 mM NaCl, 1% NP40, 1% sodium deoxycholate, 0.1% SDS, 1 mM EDTA pH 7.6) supplemented with 1× protease/phosphatase inhibitor cocktail (Cell Signaling). For co-immunoprecipitation studies, cells were lysed in NP-40 buffer

(150 mM NaCl, 1% NP-40, 50 mM Tris-Cl pH 8.0) supplemented with 1× protease/ phosphatase inhibitor cocktail (Cell Signaling). For RNase treatment, 3.33 μg of RNase A (Thermo-Fisher) was added to 1000 μg of protein lysate and incubated at 25°C for 10 minutes. Lysates were incubated on ice for 30 minutes and then cleared by spinning at 10,000 RPM for 10 minutes at 4°C. Supernatants were incubated with GFP-Trap agarose beads (Chromotek) for 2 hours at 4°C or FLAG agarose beads at 4°C overnight. Beads were washed three times with RIPA or NP-40 lysis buffer afterward for YB-1 phosphorylation and co-immunoprecipitation studies respectively. Bound proteins were eluted with 4× Laemmli Sample Buffer (BioRad) and visualized by SDS-PAGE on nitrocellulose membranes followed by immunoblot analysis. A portion of each protein lysate input was run concurrently to measure total expression for each protein.

Cell viability assay—Cells were seeded in triplicate in a 96-well white plates with a clear bottom at 2,000–8,000 cells per well, and measured every other day using Cell Titer Glo reagent (Promega). Plates were read on a Tecan Infinite M1000 Microplate reader, and results were analyzed in GraphPad Prism 9 software.

Caspase Glo—Cells were seeded in triplicate in a 96-well white plate with a clear bottom at 500–2,000 cells per well. ErbB2-BrM2 cells were treated with DMSO, 10 μM GNF5, or 10 μM ABL001 for 48 hours. For a positive control, cells were treated with 1 μM staurosporine (Sigma-Aldrich) for 4.5 hours. Caspase activity was measured by Caspase-Glo 3/7 reagent (Promega). Plates were read on a Tecan Infinite M1000 Microplate reader, and results were analyzed in GraphPad Prism 9 software.

Nuclear/cytoplasmic cell fractionation—Fractionation of cells was performed following the REAP cell fractionation method as previously described (Suzuki et al., 2010). Briefly, HCC1954-LCC1 cells were plated into 10 cm dishes and treated with DMSO or 10 μM GNF5 for 48 hours. Cells were harvested in ice-cold PBS and centrifuged for 10 seconds in a tabletop centrifuge. The supernatant was removed and cells were lysed and triturated in ice-cold 0.1% NP-40 in PBS. A portion of the lysate was removed and used for the whole cell lysate fraction. The remaining lysate was centrifuged for 10 seconds. A portion of the supernatant was removed and designated the cytosolic fraction. The remaining supernatant was removed and the pellet was washed with ice-cold 0.1% NP40. The samples were centrifuged for 10 seconds and the supernatant was removed. The pellet was resuspended in 1× Laemmli buffer and designated the nuclear fraction. Laemmli sample buffer was added to the whole cell lysate and cytoplasmic fractions. The nuclear and whole cell lysate fractions were sonicated twice for 5 seconds on ice. The samples were boiled for 1 minute prior to immunoblot analysis.

2D colony formation assay—100 ErbB2-BrM2 cells were seeded into a 6-well plate. Cells were treated with DMSO, 10 μM GNF5, or 10 μM ABL001 for 7 days. The media and drug were replenished every 2 days. For CRISPR KO colony formation assays, 200 ErbB2-BrM2 control and ABL1/2 KO cells were seeded into a 6-well plate. On day 7, the media was removed and the cells were washed 3× with PBS. The cells were fixed in 100% ice-cold methanol for 10 minutes. The cells were stained with 0.5% crystal violet in 25%

methanol for 20 minutes. The plates were rinsed with water and dried overnight. The next day, the plates were imaged and the colonies destained for 20 minutes using 10% acetic acid. The absorbance was measured at 590 nm using a Tecan Infinite M1000 Microplate reader (adapted from (Kim et al., 2019)).

Flow cytometry—ErbB2-BrM2 and SUM190-BrM cells were treated with DMSO or 10 μM GNF5 for 48 hours. Following treatment, 1,000,000 cells were washed once with PBS. The cells were resuspended in 50 μL blocking buffer (PBS+ 2% HI FBS (Life Technologies) + 0.05% sodium azide+ BD Fc Block (BD Biosciences)). The cells were incubated for 5 minutes at 4°C. 50 μL of blocking buffer and 5 μL PE Rat anti-Mouse ErbB2 (R&D FAB6744P) were added to stain ErbB2-BrM2 samples. 50 μL of blocking buffer and 5 μL APC/Fire750 anti-human HER2 (BioLegend #324422) were added to stain SUM190-BrM samples. The cells were incubated for 30 min at 4°C in the dark. The cells were washed twice with FACS buffer (PBS+2% HI FBS+ 0.05% sodium azide). The cells were resuspended in 300 μL FACS buffer. The samples were run on a BD FACS Canto flow cytometer. The data was analyzed using FlowJo Version 10.

Immunoblotting—Cells were lysed in RIPA buffer (50 mM Tris HCl, 150 mM NaCl, 1% NP40, 1% sodium deoxycholate, 0.1% SDS, 1 mM EDTA pH 7.6) supplemented with 1× protease/phosphatase inhibitor cocktail (Cell Signaling). Cell lysates were rotated at 4°C for 30 minutes followed by centrifugation at 15,000 RPM for 15 minutes at 4°C. The cell debris was discarded and the lysates were quantified using the DC Protein Assay (Bio-Rad). Proteins were separated using 7.5% polyacrylamide gels and transferred to 0.2 μm nitrocellulose membranes (Bio-Rad). The membranes were stained with 0.1% Ponceau before blocking. The membranes were blocked in 5% milk for 1 hour and probed with HER2 (Cell Signaling #2165, 1:10,000), HER2 (Cell Signaling #4290, 1:1000), p-CrkL (Tyr207) (Cell Signaling #3181, 1:2000), CrkL (Santa Cruz sc-319, 1:1000), GAPDH (Santa Cruz sc-32233, 1:5000), ABL1 (BD Biosciences #55448, 1:1000), ABL2 (Abnova H00000027-M03, 1:1000), SSB (Cell Signaling #5034, 1:1000), YB-1 (Santa Cruz sc-101198, 1:1000), YB-1 (Cell Signaling #9744, 1:1000), GFP (Cell Signaling #2956, 1:2000–1:5000), phospho-ABL1 (Y245) (Cell Signaling #2868, 1:1000), Phospho-Tyrosine (Sigma #05–321, 1:1000), FLAG (Sigma #F1804,1:1000), Lamin B1 (Cell Signaling #13435, 1:1000), SOX2 (Cell Signaling#3579, 1:1000), MMP9 (Cell Signaling #13667, 1:1000) AXL (Cell Signaling #8861, 1:1000), AXL (Santa Cruz sc-166269, 1:1000), L1CAM (Cell Signaling #89861, 1:1000), SREBP1 (Novus NB100–2215SS, 1:1000), p-STAT3 (Y705) (Cell Signaling #9145, 1:1000), and STAT3(Cell Signaling #4904, 1:1000) primary antibodies in 5% milk or 3% bovine serum albumin at 4°C overnight. The membranes were probed with Peroxidase AffiniPure Goat anti Mouse IgG (H + L) (Jackson Immunoresearch, 1:2000–1:5000), Peroxidase AffiniPure Goat anti Rabbit IgG (H + L) (Jackson Immunoresearch, 1:2000–1:10,000), or TidyBlot Western Blot Detection Reagent:HRP (BioRad, 1:500) secondary antibodies in 5% milk for 1 hour at room temperature. Immunoblots were visualized using SuperSignal West PLUS Chemiluminescent Substrate developing solution (Thermo Fisher) and imaged using X-ray film.

Intracranial injections—All animal experiments were conducted in accordance with protocols approved by the Duke University Division of Laboratory Animal Resources Institutional Animal Care and Use Committee (IACUC). All mice used for immunodeficient studies were 8–12 week female athymic nu/nu mice (Jackson Laboratory). The day prior to HCC1954-LCC1 intracranial injections, all mice were injected intraperitoneally with 50 uL of anti-asialo GM1 (Fujifilm Wako). The mice were injected with anti-asialo GM1 every 5 days throughout the experiment. For intracranial injections, mice were anesthetized with 5% isoflurane. Breast cancer brain metastatic cells suspended in 5 uL of PBS were injected 2 mm to the right of the bregma using a stereotactic frame. Mice were injected with 100,000 HCC1954-LCC1 cells for GNF5 treatment studies and 50,000 HCC1954-LCC1 cells for YB-1 knockdown studies. Mice were injected with 25,000 SUM190-BrM cells for YB-1 knockdown studies. For immunocompetent studies, FVB mice (Jackson Laboratory) were injected intracranially with 500 ErbB2-BrM2 cells. Animals were monitored until recovery from anesthesia. To measure tumor burden, the mice were injected with Xenolight D-luciferin (PerkinElmer) and imaged using the IVIS Lumina XR bioluminescent imager. Bioluminescent images were analyzed using the Living Image software. For pharmacologic studies, mice bearing brain metastases were divided into treatment groups at Day 7–10 post-injection. GNF5 and ABL001 were prepared as a 10 mg/mL suspension in 0.5% methylcellulose/0.5% Tween-80. For HCC1954-LCC1 study, mice were treated with vehicle or 100 mg/kg GNF5 twice daily by oral gavage. For ErbB2-BrM2 study, mice were treated with vehicle or 100 mg/kg ABL001 once daily by oral gavage (Wylie et al., 2017).

Immunofluorescence—After euthanasia, the mouse was perfused with 0.25 mg/mL heparin in ice-cold PBS. Then, the mouse was perfused with ice-cold 4% paraformaldehyde (PFA). The brain was dissected and transferred to 4% PFA for 2 hours on ice. The brains were transferred to 20% sucrose in PBS and incubated overnight at 4°C. The next day, the brains were transferred to 30% sucrose in PBS and incubated overnight at 4°C. The brains were embedded in OCT and 10 μm sections were cut. The brain sections were washed 2× in TBS and blocked in 5% normal goat serum in TBST for 1 hour at room temperature. The brains were stained overnight at 4°C with HER2 (Santa Cruz sc-33684, 1:250). The sections were washed 3× with TBST and incubated with secondary antibody Alexa Fluor 633 Goat Anti Mouse IgG (H + L) (Thermo Fisher, 1:250) for 1 hour in the dark at room temperature. The slides were washed 3× with TBST. The sections were stained with Hoescht 33342 (5 μg/mL) for 10 minutes at room temperature in the dark. The sections were washed 3× with TBST and 1× with TBS. The cover slips were mounted using Dako aqueous mounting medium (Dako). The sections were imaged using a Leica SP8 upright confocal microscope.

RT-qPCR—RNA was isolated from cell culture plates using the RNAspin Mini Kit (GE Healthcare). cDNA was prepared using oligo(dT) primers (Invitrogen), RNase OUT (Invitrogen), and M-MLV reverse transcriptase (Invitrogen). Primers used for RT-qPCR are listed in Table S1. RT-qPCR was performed using iTAQ Universal SYBR Green mix (Bio-Rad) on a Bio-Rad CFX384 machine. Data was analyzed using the Bio-Rad CFX Maestro software. *GAPDH* was used as the house keeping gene for analysis.

Polysome fractionation—ErbB2-BrM2 cells were treated with DMSO, 10 μM GNF5, or 10 μM DPH for 48 hours. The cells were lysed in a modified RIPA buffer (50 mM Tris HCl pH 7.6, 150 mM NaCl, 5 mM MgCl$_2$, 1% NP40, 1% sodium deoxycholate, 1X protease/phosphatase inhibitor cocktail (Cell Signaling), 1 mM DTT (Invitrogen), 40 U/mL RNase OUT (Invitrogen), 0.2 mM cycloheximide) and centrifuged at 12,000 × g for 10 minutes at 4°C. The clarified lysate was overlaid on a sucrose gradient (15–50% sucrose in 200 mM KCl, 15 mM MgCl$_2$, 25 mM K-HEPES, pH 7.2–7.4, 0.2 mM cycloheximide, 1 mM DTT, and 10 U/mL RNase OUT) and centrifuged at 35,000 RPM for 3 hours at 4°C. Twenty 0.5 mL fractions were collected using a gradient fractionator with continuous monitoring of UV254 nm absorbance. The RNA was isolated from the fractions using TRIzol reagent (Thermo-Fisher) according to the manufacturer's protocol. cDNA was prepared using 10 uL of RNA and RT-qPCR was performed for *ACTB* and *ERBB2* according to the protocol above.

[^{35}S]-methionine/cysteine pulse—HCC1954-LCC1 and ErbB2-BrM2 cells were treated with DMSO, 10 μM GNF5, or 10 μM DPH for 48 hours. HCC1954-LCC1 shScr, shAA, shNTC, and shYB-1 cells were prepared according to the lentiviral transduction protocol above. The cells were incubated in methionine-free media (DMEM (Life Technologies #21013024), 10% dialyzed FBS (Sigma #F0392)) for 15–30 minutes at 37°C. Cycloheximide-control cells were treated with 100 ug/mL cycloheximide prior to radiolabelling. The cells were pulsed with [^{35}S]-methionine/cysteine (150 μCi/mL) for 30 minutes. Following radiolabelling, cells were treated with 100 ug/mL cycloheximide for 10 minutes at 37°C. The cells were lysed in RIPA+1 × protease/phosphatase inhibitor cocktail (Cell Signaling). The lysates were rotated at 4°C for 30 minutes and centrifuged at 15,000 RPM for 15 minutes at 4°C. The supernatant was used for immunoprecipitation. The lysates were pre-cleared with Rabbit IgG (Novus) or Mouse IgG (Santa Cruz) and A/G-Agarose beads (Santa Cruz). The lysates were incubated with Rabbit IgG (Novus), Mouse IgG (Santa Cruz), HER2 (Santa Cruz, sc-33684, 1 ug) or HER2 (29D8) antibody (Cell Signaling, 1:100) at 4°C overnight. The lysates were incubated with A/G-Agarose beads for 2 hours at 4°C. The beads were washed 3× with RIPA and the proteins were eluted in 2× sample buffer (Bio-Rad). The radioactivity was measured using a liquid scintillation counter. The counts per minute (CPM) for each sample was normalized to the amount of input protein used for the immunoprecipitation (μg). The following formula was used to calculate the amount of radio-labelled HER2 in each sample.

$$\left(\frac{CPM}{\mu g\ protein}\right)_{HER2} = \left(\frac{CPM}{\mu g\ protein}\right)_{sample} - \left(\frac{CPM}{\mu g\ protein}\right)_{CHX\ Control}$$

Phosphorimaging—The samples were run on a 4–15% gel (Bio-Rad). The gel was fixed in 10% acetic acid, 50% methanol for 1 h at room temperature. The gel was rinsed 2× with deionized water. The gel was incubated in deionized water for 30 min at room temperature 2×. The gel was dried at 70°C overnight. The gel was exposed to the phosphor screen and imaged using a GE Amersham Typhoon.

Calculation of HER2 half-life—Cells were treated with DMSO or 10 μM GNF5 and 20 ug/mL cycloheximide (Sigma) for 0, 2, 4, 8, 24, and 48 hours. The cell lysates were prepared and immunoblotting for HER2 and GAPDH was performed as described above. The levels of HER2 were normalized to GAPDH and plotted over time in GraphPad Prism 9. A nonlinear best fit curve was plotted for one-phase decay.

Proteasomal inhibition—Cells were treated with DMSO or 10 μM GNF5 for 48 h 1 μM MG132 was added to the cells during the last 24 hours of drug treatment. The cell lysates were prepared and immunoblotting was performed as described above.

Preparation of mRNA probes for pulldown—The pBABEpuro-ERBB2 plasmid was a gift from Matthew Meyerson (Addgene plasmid #40978) (Greulich et al., 2012). RNA was isolated from HCC1954-LCC1 cells using the RNASpin Mini Kit (GE Healthcare). cDNA was prepared using oligo(dT) primers (Invitrogen), RNase OUT (Invitrogen), and Maxima reverse transcriptase (Thermo Fisher). The 5′ and-3′ UTR of *ERBB2* were PCR amplified using DreamTaq DNA polymerase (Thermo Fisher). Primers for PCR amplification were designed to include the T7 promoter on the 5′ end. 5′ UTR PCR primers were: Forward 5′-AGTAATACGACTCACTATAGGGATTCCCCTCCATTGGGACCG-3′, Reverse 5′-GGTGCTCACTGCGGCTCCGG-3′. 3′ UTR PCR primers were: Forward 5′-AGTAATACGACTCACTATAGGGACCAGAAGGCCAAGTCCG-3′, Reverse 5′-GTTTTCCAAAATATATTTGCAAATGGACAAAGTGGGTGTGG-3′. The PCR products were separated by gel electrophoresis and isolated using the QIAquick Gel Extraction Kit (Qiagen). The coding region of the *ERBB2* mRNA was PCR amplified from pBABEpuro-ERBB2 using Q5 High-Fidelity Master Mix (New England BioLabs). Primers for PCR amplification were designed to include the T7 promoter at the 5′ end. Primers for PCR amplification of the coding region were: Forward 5′-AGTAATACGACTCACTATAGGGATGGAGCTGGCGGCCTTG-3′, Reverse 5′-TCACACTGGCACGTCCAGACC-3′ 5′-TCACACTGGCACGTCCAGACCC-3′. The PCR products were separated by gel electrophoresis and isolated using the QIA quick Gel Extraction Kit (Qiagen). *In vitro* transcription was performed using the PCR products for 5′ UTR, 3′ UTR, and coding region of *ERBB2* and the MEGAscript T7 Transcription kit (Thermo Fisher).

RNA protein pulldown—HCC1954-LCC1 cells were treated with DMSO or 10 μM GNF5 for 48 h 5′ UTR, 3′UTR and coding *ERBB2* mRNA was biotinylated using the Pierce RNA 3′ End Desthiobiotinylation kit (Thermo Fisher). RNA binding proteins were immunoprecipitated using the Pierce Magnetic RNA-Protein Pull-Down kit (Thermo Fisher). Immunoprecipitated proteins were washed 3× with 1% NP-40, 150 mM NaCl, 25 mM Tris (pH 7.5). Proteins were eluted in 2% SDS, 25 mM Tris (pH 7.5), 5 mM DTT, and 5 mM free biotin at 80°C for 10 min. Proteins were run on a 4–15% polyacrylamide gel (BioRad) and the gel was silver stained using the Pierce Silver Stain for Mass Spectrometry Kit (Thermo Fisher). Bands were excised and identified by LC-MS/MS by the Duke Center for Genomic and Computational Biology.

LC-MS/MS proteomics analysis—For gel band analysis, SDS-PAGE gel bands were subjected to reduction, alkylation, and in-gel tryptic digestion as described here: https://genome.duke.edu/sites/genome.duke.edu/files/In-gelDigestionProtocolrevised_0.pdf. Digested peptides were lyophilized to dryness and resuspended in 12 uL of 0.2% formic acid/2% acetonitrile. Each sample was subjected to chromatographic separation on a Waters NanoAquity UPLC equipped with a 1.7 μm HSS T3 C18 75 μm I.D. X 250 mm reversed-phase column (NanoFlow data). The mobile phase consisted of (A) 0.1% formic acid in water and (B) 0.1% formic acid in acetonitrile. 3 μL was injected and peptides were trapped for 3 min on a 5 μm Symmetry C18 180 μm I.D. X 20 mm column at 5 μL/min in 99.9% A. The analytical column was then switched in-line and a linear elution gradient of 5% B to 40% B was performed over 30 min at 400 nL/min. The analytical column was connected to a Fusion Lumos mass spectrometer (Thermo) through an electrospray interface operating in a data-dependent mode of acquisition. The instrument was set to acquire a precursor MS scan from m/z 375–1500 at R = 120,000 (target AGC 2×10^5, max IT 50 ms) with MS/MS spectra acquired in the ion trap (target AGC 5×10^3, max IT 100 ms). For all experiments, HCD energy settings were 30v and a 20 s dynamic exclusion was employed for previously fragmented precursor ions. Raw LC-MS/MS data files were processed in Proteome Discoverer (Thermo Scientific) and then submitted to independent Mascot searches (Matrix Science) against a Human protein database containing both forward (20260 entries) and reverse entries of each protein. Search tolerances were 5 ppm for precursor ions and 0.8 Da for product ions using trypsin specificity with up to two missed cleavages. Carbamidomethylation (+57.0214 Da on C) was set as a fixed modification, whereas oxidation (+15.9949 Da on M) and deamidation (+0.98 Da on NQ) were considered dynamic mass modifications. All searched spectra were imported into Scaffold (v4.4, Proteome Software) and scoring thresholds were set to achieve a peptide false discovery rate of 1% using the PeptideProphet algorithm. Data was visualized using Scaffold 4 software.

RNA immunoprecipitation—Cells were treated with DMSO, 10 μM GNF5, or 10 μM ABL001 for 48 or 72 h. RNA immunoprecipitation was performed using the MagnaRIP RNA-binding protein Immunoprecipitation kit (Sigma) according to the manufacturer's instructions. 5 ug of YB-1 antibody (Santa Cruz sc-101198) or mouse IgG (Santa Cruz) was used for the immunoprecipitation. 10 uL of RNA was used for the cDNA synthesis and RT-qPCR was performed on input and immunoprecipitation samples as detailed above.

CLIP-sequencing analysis—YB-1 HITS-CLIP dataset for long RNA species (GEO: GSE63604) was analyzed using the standard approach to identify YB-1 binding sites (Goodarzi et al., 2015; Shah et al., 2017). Briefly, reads were filtered and the 3′ adaptor sequence was trimmed. The duplicates were collapsed and 5′ degenerate barcode was removed. The reads were aligned to the human genome (hg19; (Langmead and Salzberg, 2012)). Unique CLIP tags were obtained by collapsing PCR duplicates. The genomic distribution of CLIP tags was obtained and visualized using the Integrative Genomics Viewer (Robinson et al., 2011). Galaxy (usegalaxy. org) was used to quantify the number of CLIP tags across each gene. To define background YB-1 binding, the average number of

CLIP tags across 100 randomly selected genes was quantified (103 CLIP tags). Transcripts with >103 CLIP tags were defined as 'YB-1 binding targets'.

HER2 mRNA stability—Cells were treated with DMSO or 10 μM GNF5 for 48 h 5 ug/mL actinomycin-D was added during the last 2, 4, 8, and 12 h of drug treatment. The RNA was isolated, cDNA was prepared, and RT-qPCR was performed as described above.

***In vitro* kinase assay—**1.0 μg of recombinant His-YB-1 (Novus Biologicals) was added to kinase buffer (25 mM Tris HCl pH 7.5, 20 mM $MgCl_2$, 1 mM DTT, 25 mM β-glycerol phosphate, 0.5 mM Na_3VO_4, 100 μM ATP). 1.0 μg of recombinant GST-ABL1 (Pro137-Ser554) (Sino Biological) was added to His-YB-1 and the reaction was incubated at 37°C for 30 min. The reaction stopped by adding 4× Laemmli buffer and the samples were prepared for immunoblot analysis.

Breast cancer patient analysis—Breast cancer patient microarray data were analyzed using the KMplot analysis tool (kmplot.com) (Gyorffy et al., 2010). HER2+ breast cancer patients were stratified by quartile (n = 451 total patients across all cohorts). Affimetrix identifier for YB-1 was 216,940_x_at. Mutual exclusivity analysis was performed with cBioPortal using the Metastatic Breast Cancer Project, INSERM Metastatic Breast Cancer dataset, TCGA Breast Invasive Carcinoma dataset, Sanger Breast Invasive Carcinoma dataset, Broad Breast Invasive Carcinoma dataset, British Columbia Breast Invasive Carcinoma dataset, SMC Breast Cancer dataset, MSKCC Breast Cancer dataset, METABRIC breast cancer dataset, and MSK breast cancer dataset (n = 6513 patients) (Banerji et al., 2012; Curtis et al., 2012; Kan et al., 2018; Lefebvre et al., 2016; Nixon et al., 2019; Pereira et al., 2016; Razavi et al., 2018; Shah et al., 2012; Stephens et al., 2012). Patients with mRNA expression data and Z score threshold ±2.0 were included. Mutual exclusivity analysis was performed on cBioPortal using default settings and results were plotted using Graphpad Prism 9 software.

QUANTIFICATION AND STATISTICS ANALYSIS

Immunoblots and immunofluorescence images were quantified using ImageJ (Schneider et al., 2012). HER2 expression measured in immunofluorescence images were normalized to the number of nuclei in the tumors. All statistics were performed using the Graphpad Prism 9 software. To calculate the p value for Kaplan-Meier survival curves, a Mantel-Cox log rank test was performed. For statistical comparisons between two groups, a student's t-test (unpaired, two-tailed) was performed. Statistical comparisons of more than two groups were conducted using an ANOVA followed by Bonferroni's or Holm-Šidák post-hoc testing. Outliers were detected using Grubb's test. For all tests, a p value <0.05 was considered significant. All figures show mean ± SEM. Statistical analysis and the number of biological replicates (n) for specific experiments are indicated in the corresponding figure legends. For mouse experiments, mice were divided evenly between treatment groups so that the tumor burden was not significantly different between groups at the start of treatment as measured by a student's t-test (unpaired, two-tailed).

Supplementary Material

Refer to Web version on PubMed Central for supplementary material.

ACKNOWLEDGMENTS

REFERENCES

Andrulis IL, Bull SB, Blackstein ME, Sutherland D, Mak C, Sidlofsky S, Pritzker KP, Hartwick RW, Hanna W, Lickley L, et al. (1998). neu/erbB-2 amplification identifies a poor-prognosis group of women with node-negative breast cancer. Toronto Breast Cancer Study Group. J. Clin. Oncol. 16, 1340–1349. [PubMed: 9552035]

Aversa C, Rossi V, Geuna E, Martinello R, Milani A, Redana S, Valabrega G, Aglietta M, and Montemurro F (2014). Metastatic breast cancer subtypes and central nervous system metastases. Breast 23, 623–628. [PubMed: 24993072]

Banerji S, Cibulskis K, Rangel-Escareno C, Brown KK, Carter SL, Frederick AM, Lawrence MS, Sivachenko AY, Sougnez C, Zou L, et al. (2012). Sequence analysis of mutations and translocations across breast cancer subtypes. Nature 486, 405–409. [PubMed: 22722202]

Baraibar I, Mezquita L, Gil-Bazo I, and Planchard D (2020). Novel drugs targeting EGFR and HER2 exon 20 mutations in metastatic NSCLC. Crit. Rev. Oncol. Hematol. 148, 102906. [PubMed: 32109716]

Bargou RC, Jürchott K, Wagener C, Bergmann S, Metzner S, Bommert K, Mapara MY, Winzer KJ, Dietel M, Dörken B, and Royer HD (1997). Nuclear localization and increased levels of transcription factor YB-1 in primary human breast cancers are associated with intrinsic MDR1 gene expression. Nat. Med. 3, 447–450. [PubMed: 9095180]

Burton EA, Plattner R, and Pendergast AM (2003). Abl tyrosine kinases are required for infection by Shigella flexneri. EMBO J. 22, 5471–5479. [PubMed: 14532119]

Chang G, Shi L, Ye Y, Shi H, Zeng L, Tiwary S, Huse JT, Huo L, Ma L, Ma Y, et al. (2020). YTHDF3 Induces the translation of m(6)A-enriched gene transcripts to promote breast cancer brain metastasis. Cancer Cell 38, 857–871.e7. [PubMed: 33125861]

Chislock EM, and Pendergast AM (2013). Abl family kinases regulate endothelial barrier function in vitro and in mice. PLoS One 8, e85231. [PubMed: 24367707]

Chislock EM, Ring C, and Pendergast AM (2013). Abl kinases are required for vascular function, Tie2 expression, and angiopoietin-1-mediated survival. Proc. Natl. Acad. Sci. USA 110, 12432–12437. [PubMed: 23840065]

Chowdhury B, Porter EG, Stewart JC, Ferreira CR, Schipma MJ, and Dykhuizen EC (2016). PBRM1 regulates the expression of genes involved in Metabolism and cell Adhesion in renal clear cell carcinoma. PLoS One 11, e0153718. [PubMed: 27100670]

Curtis C, Shah SP, Chin SF, Turashvili G, Rueda OM, Dunning MJ, Speed D, Lynch AG, Samarajiwa S, Yuan Y, et al. (2012). The genomic and transcriptomic architecture of 2, 000 breast tumours reveals novel subgroups. Nature 486, 346–352. [PubMed: 22522925]

Doyle T, Moncorgé O, Bonaventure B, Pollpeter D, Lussignol M, Tauziet M, Apolonia L, Catanese MT, Goujon C, and Malim MH (2018). The interferon-inducible isoform of NCOA7 inhibits endosome-mediated viral entry. Nat. Microbiol. 3, 1369–1376. [PubMed: 30478388]

Ebright RY, Lee S, Wittner BS, Niederhoffer KL, Nicholson BT, Bardia A, Truesdell S, Wiley DF, Wesley B, Li S, et al. (2020). Deregulation of ribosomal protein expression and translation promotes breast cancer metastasis. Science 367, 1468–1473. [PubMed: 32029688]

El-Naggar AM, Veinotte CJ, Cheng H, Grunewald TGP, Negri GL, Somasekharan SP, Corkery DP, Tirode F, Mathers J, Khan D, et al. (2015). Translational activation of HIF1alpha by YB-1 promotes sarcoma metastasis. Cancer Cell 27, 682–697. [PubMed: 25965573]

Evdokimova V, Tognon C, Ng T, Ruzanov P, Melnyk N, Fink D, Sorokin A, Ovchinnikov LP, Davicioni E, Triche TJ, and Sorensen PHB (2009). Translational activation of snail1 and other developmentally regulated transcription factors by YB-1 promotes an epithelial-mesenchymal transition. Cancer Cell 15, 402–415. [PubMed: 19411069]

Goodarzi H, Liu X, Nguyen HCB, Zhang S, Fish L, and Tavazoie SF (2015). Endogenous tRNA-derived fragments suppress breast cancer progression via YBX1 displacement. Cell 161, 790–802. [PubMed: 25957686]

Goyette MA, Duhamel S, Aubert L, Pelletier A, Savage P, Thibault MP, Johnson RM, Carmeliet P, Basik M, Gaboury L, et al. (2018). The receptor tyrosine kinase AXL is required at multiple steps of the metastatic cascade during HER2-positive breast cancer progression. Cell Rep. 23, 1476–1490. [PubMed: 29719259]

Greulich H, Kaplan B, Mertins P, Chen TH, Tanaka KE, Yun CH, Zhang X, Lee SH, Cho J, Ambrogio L, et al. (2012). Functional analysis of receptor tyrosine kinase mutations in lung cancer identifies oncogenic extracellular domain mutations of ERBB2. Proc. Natl. Acad. Sci. USA 109, 14476–14481. [PubMed: 22908275]

Gril B, Paranjape AN, Woditschka S, Hua E, Dolan EL, Hanson J, Wu X, Kloc W, Izycka-Swieszewska E, Duchnowska R, et al. (2018). Reactive astrocytic S1P3 signaling modulates the blood-tumor barrier in brain metastases. Nat. Commun. 9, 2705. 10.1038/s41467-018-05030-w. [PubMed: 30006619]

Gu JJ, Rouse C, Xu X, Wang J, Onaitis MW, and Pendergast AM (2016). Inactivation of ABL kinases suppresses non-small cell lung cancer metastasis. JCI Insight 1, e89647. [PubMed: 28018973]

Györffy B, Lanczky A, Eklund AC, Denkert C, Budczies J, Li Q, and Szallasi Z (2010). An online survival analysis tool to rapidly assess the effect of 22, 277 genes on breast cancer prognosis using microarray data of 1, 809 patients. Breast Cancer Res. Treat. 123, 725–731. [PubMed: 20020197]

Hoj JP, Mayro B, and Pendergast AM (2019). A TAZ-AXL-ABL2 feed-forward signaling Axis promotes lung adenocarcinoma brain metastasis. Cell Rep. 29, 3421–3434.e8. [PubMed: 31825826]

Hulsbergen AFC, Claes A, Kavouridis VK, Ansaripour A, Nogarede C, Hughes ME, Smith TR, Brastianos PK, Verhoeff JJC, Lin NU, and Broekman MLD (2020). Subtype switching in breast cancer brain metastases: a multicenter analysis. Neuro Oncol. 22, 1173–1181. [PubMed: 31970416]

Jiang D, Qiu T, Peng J, Li S, Ren W, Ren W, Yang C, Wen Y, Chen CH, Sun J, et al. (2022). YB-1 is a positive regulator of KLF5 transcription factor in basal-like breast cancer. Cell Death Differ. 29, 1283–1295. [PubMed: 35022570]

Johnson TG, Schelch K, Mehta S, Burgess A, and Reid G (2019). Why Be one protein when you can affect many? The multiple roles of YB-1 in lung cancer and mesothelioma. Front. Cell Dev. Biol. 7, 293. [PubMed: 31807495]

Jungfleisch J, Nedialkova DD, Dotu I, Sloan KE, Martinez-Bosch N, Brüning L, Raineri E, Navarro P, Bohnsack MT, Leidel SA, and Díez J (2017). A novel translational control mechanism involving RNA structures within coding sequences. Genome Res. 27, 95–106. [PubMed: 27821408]

Kan Z, Ding Y, Kim J, Jung HH, Chung W, Lal S, Cho S, Fernandez-Banet J, Lee SK, Kim SW, et al. (2018). Multi-omics profiling of younger Asian breast cancers reveals distinctive molecular signatures. Nat. Commun. 9, 1725. [PubMed: 29713003]

Kim YJ, Bond GJ, Tsang T, Posimo JM, Busino L, and Brady DC (2019). Copper chaperone ATOX1 is required for MAPK signaling and growth in BRAF mutation-positive melanoma. Metallomics 11, 1430–1440. [PubMed: 31317143]

Kraus MH, Popescu NC, Amsbaugh SC, and King CR (1987). Overexpression of the EGF receptor-related proto-oncogene erbB-2 in human mammary tumor cell lines by different molecular mechanisms. EMBO J. 6, 605–610. [PubMed: 3034598]

Kurmi K, Hitosugi S, Yu J, Boakye-Agyeman F, Wiese EK, Larson TR, Dai Q, Machida YJ, Lou Z, Wang L, et al. (2018). Tyrosine phosphorylation of Mitochondrial creatine kinase 1 enhances a druggable tumor energy shuttle pathway. Cell Metab. 28, 833–847.e8. [PubMed: 30174304]

Landthaler M, Gaidatzis D, Rothballer A, Chen PY, Soll SJ, Dinic L, Ojo T, Hafner M, Zavolan M, and Tuschl T (2008). Molecular characterization of human Argonaute-containing ribonucleoprotein complexes and their bound target mRNAs. RNA 14, 2580–2596. [PubMed: 18978028]

Langmead B, and Salzberg SL (2012). Fast gapped-read alignment with Bowtie 2. Nat. Methods 9, 357–359. [PubMed: 22388286]

Lefebvre C, Bachelot T, Filleron T, Pedrero M, Campone M, Soria JC, Massard C, Lévy C, Arnedos M, Lacroix-Triki M, et al. (2016). Mutational profile of metastatic breast cancers: a retrospective analysis. PLoS Med. 13, e1002201. [PubMed: 28027327]

Leivonen SK, Sahlberg KK, Mäkelä R, Due EU, Kallioniemi O, Børresen-Dale AL, and Perälä M (2014). High-throughput screens identify microRNAs essential for HER2 positive breast cancer cell growth. Mol. Oncol. 8, 93–104. [PubMed: 24148764]

Lim JP, Shyamasundar S, Gunaratne J, Scully OJ, Matsumoto K, and Bay BH (2017). YBX1 gene silencing inhibits migratory and invasive potential via CORO1C in breast cancer in vitro. BMC Cancer 17, 201. [PubMed: 28302118]

Lin NU, Amiri-Kordestani L, Palmieri D, Liewehr DJ, and Steeg PS (2013). CNS metastases in breast cancer: old challenge, new frontiers. Clin. Cancer Res. 19, 6404–6418. [PubMed: 24298071]

Lin NU, Bellon JR, and Winer EP (2004). CNS metastases in breast cancer. J. Clin. Oncol. 22, 3608–3617. [PubMed: 15337811]

Liu L, Greger J, Shi H, Liu Y, Greshock J, Annan R, Halsey W, Sathe GM, Martin AM, and Gilmer TM (2009). Novel mechanism of lapatinib resistance in HER2-positive breast tumor cells: activation of AXL. Cancer Res. 69, 6871–6878. [PubMed: 19671800]

Malladi S, Macalinao DG, Jin X, He L, Basnet H, Zou Y, de Stanchina E, and Massagué J (2016). Metastatic latency and immune evasion through Autocrine inhibition of WNT. Cell 165, 45–60. [PubMed: 27015306]

Mauro MJ, Hochhaus A, Boquimpani C, Minami Y, Allepuz A, Polydoros F, Bédoucha V, Aimone P, and Réa D (2019). A multicenter, randomized phase III study of asciminib (ABL001) versus bosutinib in patients (pts) with chronic myeloid leukemia in chronic phase (CML-CP) previously treated with 2 tyrosine kinase inhibitors (TKIs). J. Clin. Oncol. 37, TPS7070.

Mimnaugh EG, Chavany C, and Neckers L (1996). Polyubiquitination and proteasomal degradation of the p185c-erbB-2 receptor protein-tyrosine kinase induced by geldanamycin. J. Biol. Chem. 271, 22796–22801. [PubMed: 8798456]

Muller WJ, Sinn E, Pattengale PK, Wallace R, and Leder P (1988). Single-step induction of mammary adenocarcinoma in transgenic mice bearing the activated c-neu oncogene. Cell 54, 105–115. [PubMed: 2898299]

Niikura N, Hayashi N, Masuda N, Takashima S, Nakamura R, Watanabe K.i., Kanbayashi C, Ishida M, Hozumi Y, Tsuneizumi M, et al. (2014). Treatment outcomes and prognostic factors for patients with brain metastases from breast cancer of each subtype: a multicenter retrospective analysis. Breast Cancer Res. Treat. 147, 103–112. [PubMed: 25106661]

Nixon MJ, Formisano L, Mayer IA, Estrada MV, González-Ericsson PI, Isakoff SJ, Forero-Torres A, Won H, Sanders ME, Solit DB, et al. (2019). PIK3CA and MAP3K1 alterations imply luminal A status and are associated with clinical benefit from pan-PI3K inhibitor buparlisib and letrozole in ER+ metastatic breast cancer. NPJ Breast Cancer 5, 31. [PubMed: 31552290]

Offin M, Feldman D, Ni A, Myers ML, Lai WV, Pentsova E, Boire A, Daras M, Jordan EJ, Solit DB, et al. (2019). Frequency and outcomes of brain metastases in patients with HER2-mutant lung cancers. Cancer 125, 4380–4387. [PubMed: 31469421]

Offterdinger M, and Bastiaens PI (2008). Prolonged EGFR signaling by ERBB2-mediated sequestration at the plasma membrane. Traffic 9, 147–155. [PubMed: 17956594]

Palmieri D, Bronder JL, Herring JM, Yoneda T, Weil RJ, Stark AM, Kurek R, Vega-Valle E, Feigenbaum L, Halverson D, et al. (2007). Her-2 overexpression increases the metastatic outgrowth of breast cancer cells in the brain. Cancer Res. 67, 4190–4198. [PubMed: 17483330]

Pauletti G, Godolphin W, Press MF, and Slamon DJ (1996). Detection and quantitation of HER-2/neu gene amplification in human breast cancer archival material using fluorescence in situ hybridization. Oncogene 13, 63–72. [PubMed: 8700555]

Pereira B, Chin SF, Rueda OM, Vollan HKM, Provenzano E, Bardwell HA, Pugh M, Jones L, Russell R, Sammut SJ, et al. (2016). The somatic mutation profiles of 2, 433 breast cancers refines their genomic and transcriptomic landscapes. Nat. Commun. 7, 11479. [PubMed: 27161491]

Pestalozzi BC, and Brignoli S (2000). Trastuzumab in CSF. J. Clin. Oncol. 18, 2349–2351.

Petrelli F, Tomasello G, Barni S, Lonati V, Passalacqua R, and Ghidini M (2017). Clinical and pathological characterization of HER2 mutations in human breast cancer: a systematic review of the literature. Breast Cancer Res. Treat. 166, 339–349. [PubMed: 28762010]

Plattner R, Kadlec L, DeMali KA, Kazlauskas A, and Pendergast AM (1999). c-Abl is activated by growth factors and Src family kinases and has a role in the cellular response to PDGF. Genes Dev. 13, 2400–2411. [PubMed: 10500097]

Plattner R, Koleske AJ, Kazlauskas A, and Pendergast AM (2004). Bidirectional signaling links the Abelson kinases to the platelet-derived growth factor receptor. Mol. Cell Biol. 24, 2573–2583. [PubMed: 14993293]

Priedigkeit N, Hartmaier RJ, Chen Y, Vareslija D, Basudan A, Watters RJ, Thomas R, Leone JP, Lucas PC, Bhargava R, et al. (2017). Intrinsic subtype switching and acquired ERBB2/HER2 amplifications and mutations in breast cancer brain metastases. JAMA Oncol. 3, 666–671. [PubMed: 27926948]

Razavi P, Chang MT, Xu G, Bandlamudi C, Ross DS, Vasan N, Cai Y, Bielski CM, Donoghue MTA, Jonsson P, et al. (2018). The genomic landscape of endocrine-resistant Advanced breast cancers. Cancer Cell 34, 427–438.e6. [PubMed: 30205045]

Robinson JT, Thorvaldsdóttir H, Winckler W, Guttman M, Lander ES, Getz G, and Mesirov JP (2011). Integrative genomics viewer. Nat. Biotechnol. 29, 24–26. [PubMed: 21221095]

Rostami R, Mittal S, Rostami P, Tavassoli F, and Jabbari B (2016). Brain metastasis in breast cancer: a comprehensive literature review. J. Neuro Oncol. 127, 407–414.

Sanjana NE, Shalem O, and Zhang F (2014). Improved vectors and genome-wide libraries for CRISPR screening. Nat. Methods 11, 783–784. [PubMed: 25075903]

Schneider CA, Rasband WS, and Eliceiri KW (2012). NIH Image to ImageJ: 25 years of image analysis. Nat. Methods 9, 671–675. 10.1038/nmeth.2089. [PubMed: 22930834]

Shah A, Plaza-Sirvent C, Weinert S, Buchbinder JH, Lavrik IN, Mertens PR, Schmitz I, and Lindquist JA (2020). YB-1 mediates TNF-induced pro-survival signaling by regulating NF-kappaB activation. Cancers 12, E2188. [PubMed: 32764479]

Shah A, Qian Y, Weyn-Vanhentenryck SM, and Zhang C (2017). CLIP Tool Kit (CTK): a flexible and robust pipeline to analyze CLIP sequencing data. Bioinformatics 33, 566–567. [PubMed: 27797762]

Shah SP, Roth A, Goya R, Oloumi A, Ha G, Zhao Y, Turashvili G, Ding J, Tse K, Haffari G, et al. (2012). The clonal and mutational evolution spectrum of primary triple-negative breast cancers. Nature 486, 395–399. [PubMed: 22495314]

Shen Q, Sahin AA, Hess KR, Suki D, Aldape KD, Sawaya R, and Ibrahim NK (2015). Breast cancer with brain metastases: clinicopathologic features, survival, and paired biomarker analysis. Oncol. 20, 466–473.

Shibata T, Kan H, Murakami Y, Ureshino H, Watari K, Kawahara A, Kage M, Hattori S, Ono M, and Kuwano M (2013). Y-box binding protein-1 contributes to both HER2/ErbB2 expression and lapatinib sensitivity in human gastric cancer cells. Mol. Cancer Ther. 12, 737–746. [PubMed: 23445612]

Smith-Pearson PS, Greuber EK, Yogalingam G, and Pendergast AM (2010). Abl kinases are required for invadopodia formation and chemokine-induced invasion. J. Biol. Chem. 285, 40201–40211. [PubMed: 20937825]

Srinivasan D, Kaetzel DM, and Plattner R (2009). Reciprocal regulation of Abl and receptor tyrosine kinases. Cell. Signal. 21, 1143–1150. [PubMed: 19275932]

Stemmler HJ, Schmitt M, Willems A, Bernhard H, Harbeck N, and Heinemann V (2007). Ratio of trastuzumab levels in serum and cerebrospinal fluid is altered in HER2-positive breast cancer patients with brain metastases and impairment of blood-brain barrier. Anticancer Drugs 18, 23–28. [PubMed: 17159499]

Stephens PJ, Tarpey PS, Davies H, Van Loo P, Greenman C, Wedge DC, Nik-Zainal S, Martin S, Varela I, Bignell GR, et al. (2012). The landscape of cancer genes and mutational processes in breast cancer. Nature 486, 400–404. [PubMed: 22722201]

Suzuki K, Bose P, Leong-Quong RY, Fujita DJ, and Riabowol K (2010). REAP: a two minute cell fractionation method. BMC Res. Notes 3, 294. [PubMed: 21067583]

Tanos B, and Pendergast AM (2006). Abl tyrosine kinase regulates endocytosis of the epidermal growth factor receptor. J. Biol. Chem. 281, 32714–32723. [PubMed: 16943190]

Valiente M, Obenauf AC, Jin X, Chen Q, Zhang XHF, Lee DJ, Chaft JE, Kris MG, Huse JT, Brogi E, and Massagué J (2014). Serpins promote cancer cell survival and vascular co-option in brain metastasis. Cell 156, 1002–1016. [PubMed: 24581498]

Wang J, and Pendergast AM (2015). The emerging role of ABL kinases in solid tumors. Trends Cancer 1, 110–123. [PubMed: 26645050]

Wang J, Rouse C, Jasper JS, and Pendergast AM (2016). ABL kinases promote breast cancer osteolytic metastasis by modulating tumor-bone interactions through TAZ and STAT5 signaling. Sci. Signal. 9, ra12. [PubMed: 26838548]

Wolffe AP (1994). Structural and functional properties of the evolutionarily ancient Y-box family of nucleic acid binding proteins. Bioessays 16, 245–251. [PubMed: 8031301]

Wolffe AP, Tafuri S, Ranjan M, and Familari M (1992). The Y-box factors: a family of nucleic acid binding proteins conserved from Escherichia coli to man. New Biol. 4, 290–298. [PubMed: 1622927]

Wylie AA, Schoepfer J, Jahnke W, Cowan-Jacob SW, Loo A, Furet P, Marzinzik AL, Pelle X, Donovan J, Zhu W, et al. (2017). The allosteric inhibitor ABL001 enables dual targeting of BCR-ABL1. Nature 543, 733–737. [PubMed: 28329763]

Yamazaki T, Chen S, Yu Y, Yan B, Haertlein TC, Carrasco MA, Tapia JC, Zhai B, Das R, Lalancette-Hebert M, et al. (2012). FUS-SMN protein interactions link the motor neuron diseases ALS and SMA. Cell Rep. 2, 799–806. [PubMed: 23022481]

Yang J, Campobasso N, Biju MP, Fisher K, Pan XQ, Cottom J, Galbraith S, Ho T, Zhang H, Hong X, et al. (2011). Discovery and characterization of a cell-permeable, small-molecule c-Abl kinase activator that binds to the myristoyl binding site. Chem. Biol. 18, 177–186. [PubMed: 21338916]

Yang XJ, Zhu H, Mu SR, Wei WJ, Yuan X, Wang M, Liu Y, Hui J, and Huang Y (2019). Crystal structure of a Y-box binding protein 1 (YB-1)-RNA complex reveals key features and residues interacting with RNA. J. Biol. Chem. 294, 10998–11010. [PubMed: 31160337]

Zhao J, and Xia Y (2020). Targeting HER2 alterations in non-small-cell lung cancer: a comprehensive review. JCO Precis. Oncol. 4, 411–425. [PubMed: 35050738]

Highlights

- ABL kinase inhibition decreases HER2 translation in brain metastatic cell

- YB-1 binds to *ERBB2* mRNA, and this interaction is disrupted by ABL kinase inhibitors

- ABL-mediated phosphorylation of YB-1 is required to promote HER2 translation

- ABL-YB-1 inhibition impairs outgrowth in the brain and improves overall survival
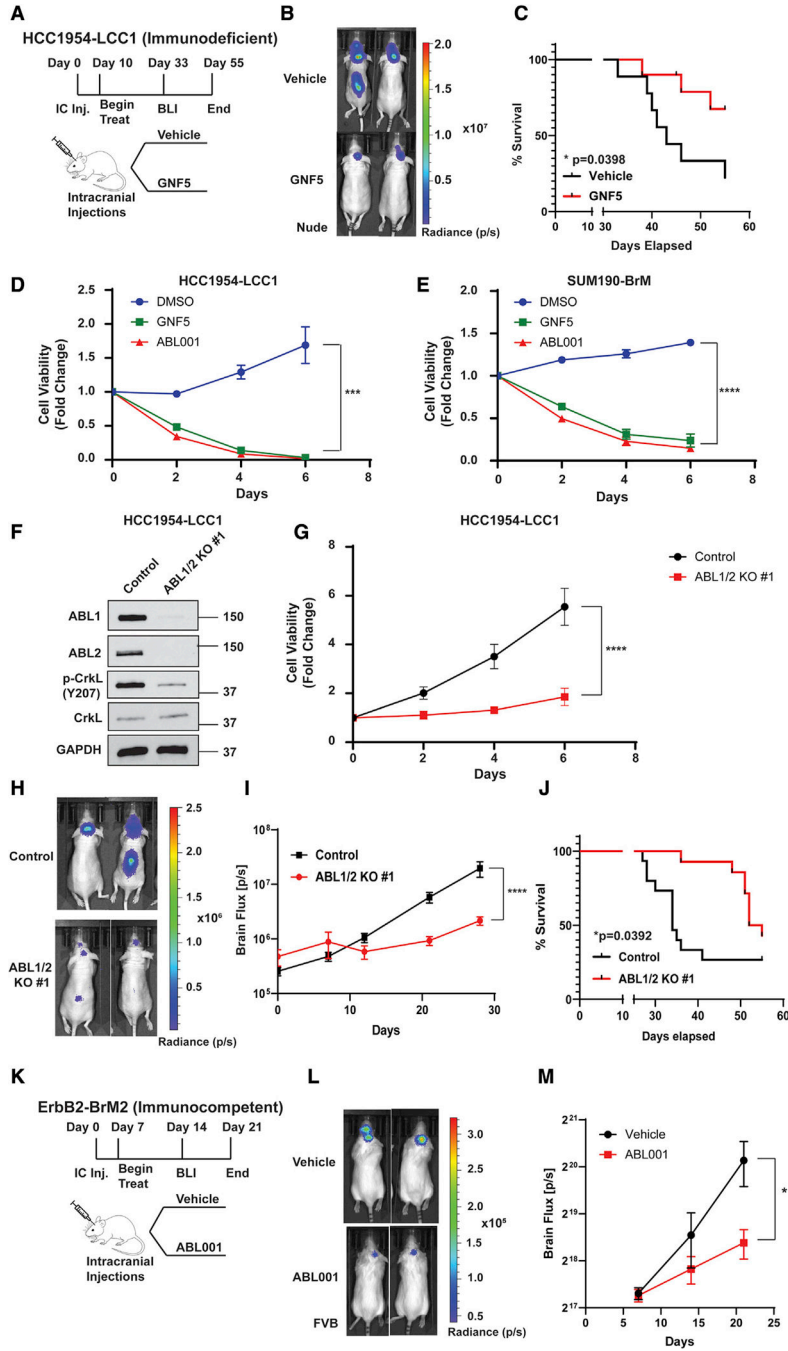
Figure 1. ABL kinase allosteric inactivation or depletion impairs outgrowth of HER2+ breast cancer brain metastatic cells and improves overall survival of tumor-bearing mice

(A–C) Nude mice were injected intracranially with HCC1954-LCC1 cells on day 0. On day 10, mice were divided between treatment groups (vehicle [n = 9] or GNF5 [n = 10]). Tumors were monitored weekly by bioluminescent imaging (BLI) until experimental endpoint (day 55).

(B) Representative BLI images on day 33.

(C) Overall survival curve of mice.

(D and E) Cell viability of HCC1954-LCC1 (D) or SUM190-BrM (E) cells treated with DMSO, 10 μM GNF5, or 10 μM ABL001 as measured by CellTiter-Glo.

(F) Immunoblots of ABL1 and ABL2 in HCC1954-LCC1 cells virally transduced with Cas9 and gRNAs targeting ABL1 and ABL2 (ABL1/2 knockout [KO] #1). Control cells are virally transduced with empty gRNA backbones (control).

(G) Cell viability of HCC1954-LCC1 ABL1/2 KO #1 and control cells as measured by CellTiter-Glo.

(H–J) Nude mice were injected intracranially with HCC1954-LCC1 control (n = 15) or ABL1/2 KO #1 (n = 15) cells.

(H) Representative BLI images of mice on day 21.

(I and J) Brain flux over time (I) and overall survival curve (J) of mice.

(K–M) FVB mice were injected intracranially with ErbB2-BrM2 cells on day 0. On day 7, mice were divided between treatment groups (vehicle or ABL001) (n = 13/group). Tumors were monitored weekly by BLI until experiment endpoint (day 21).

(L) Representative BLI images of mice on day 21 are shown.

(M) Brain flux over time in mice was measured by BLI.

Statistical analysis was performed using a repeated measures ANOVA (n = 3) or log rank (Mantel-Cox) test for survival studies. $*p < 0.05$, $***p < 0.001$, $****p < 0.0001$. Data are mean ± SEM. p/s, photons/second.
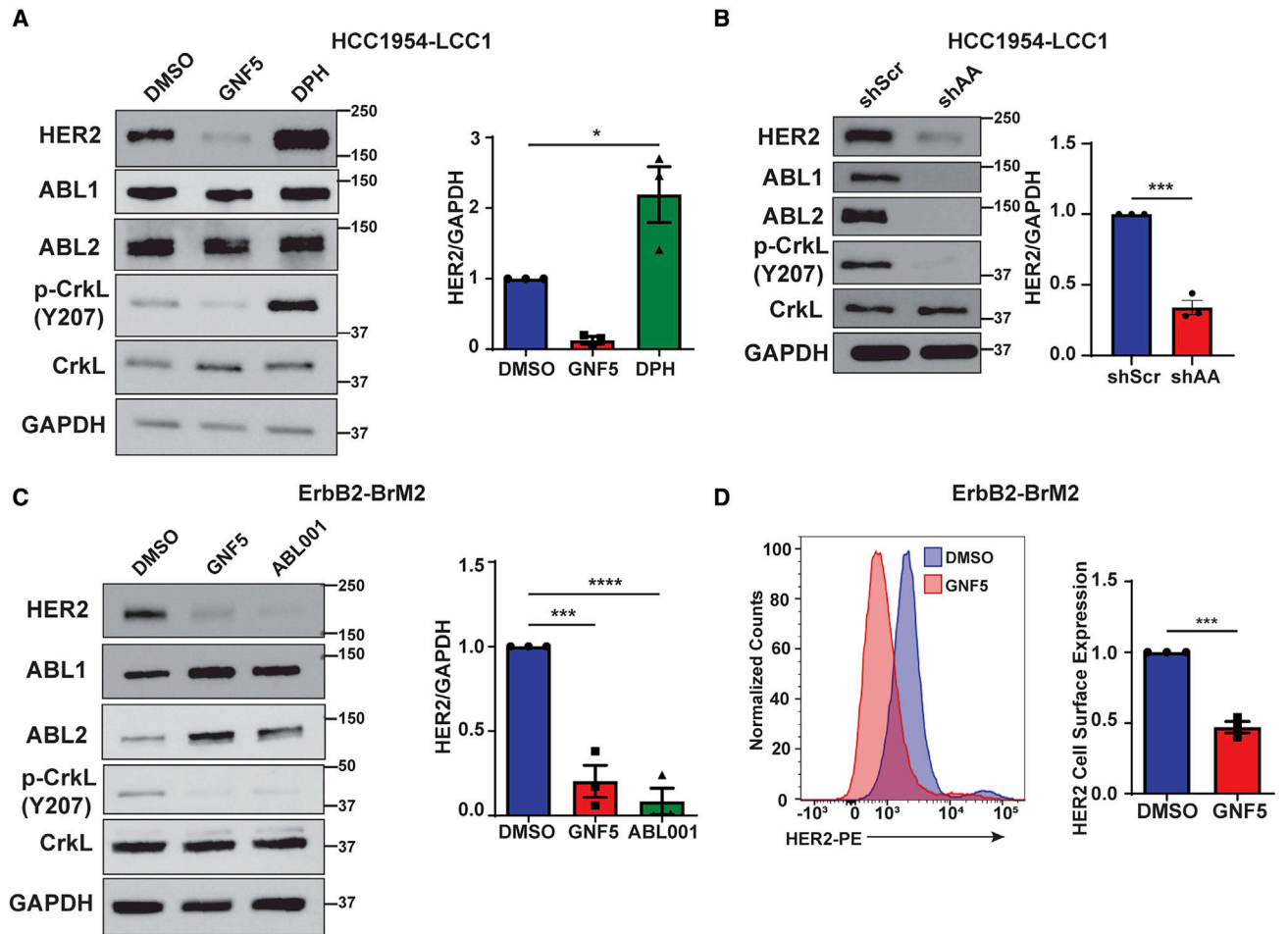
Figure 2. ABL kinase inhibition decreases HER2 protein in HER2+ breast cancer brain metastatic cells

(A) Immunoblot and quantification of HER2 in HCC1954-LCC1 cells treated with DMSO, 10 μM GNF5, or 10 μM DPH for 48 h.

(B) Immunoblot and quantification of HER2 in HCC1954-LCC1 virally transduced with shRNAs targeting ABL1 and ABL2 (shAA) or a scramble control (shScr).

(C) Immunoblot and quantification of HER2 in ErbB2-BrM2 cells treated with DMSO, 10 μM GNF5, or 10 μM ABL001 for 48 h.

(D) HER2 cell-surface levels were measured by FACS analysis of mean fluorescence intensity. ErbB2-BrM2 cells were treated with DMSO or 10 μM GNF5 for 48 h.

For immunoblots, p-CrkL serves as a marker of ABL kinase activity, and HER2 protein levels were normalized to GAPDH. Statistical analysis was performed using Student's t test and one-way ANOVA with Bonferroni's post hoc testing (n = 3). $*p < 0.05$, $***p < 0.001$, $****p < 0.0001$. Data are mean ± SEM.
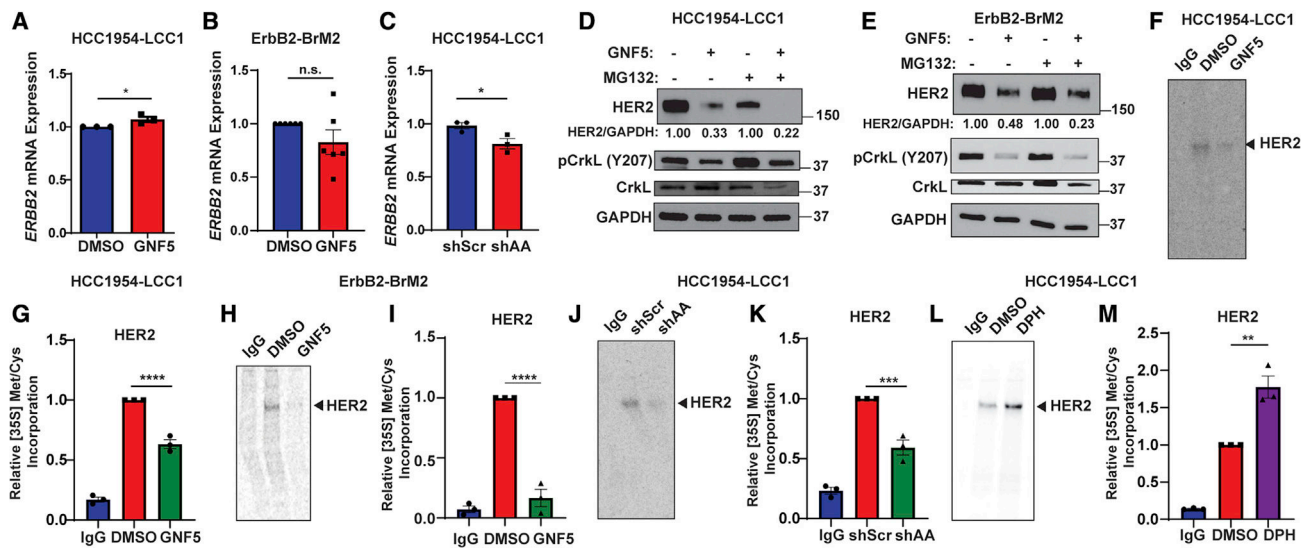
Figure 3. ABL kinases regulate HER2 translation in HER2+ brain metastatic breast cancer cells

(A and B) qRT-PCR of *ERBB2* in HCC1954-LCC1 (A) or ErbB2-BrM2 (B) cells treated with DMSO or 10 μM GNF5 for 48 h.

(C) qRT-PCR of *ERBB2* in HCC1954-LCC1 cells virally transduced with shAA or shScr.

(D and E) Immunoblot and quantification of HER2 in HCC1954-LCC1 (D) and ErbB2-BrM2 (E) cells treated with DMSO or 10 μM GNF5 for 48 h; 1 μM MG-132 was added during the last 24 h of treatment. p-CrkL serves as a marker for ABL kinase activity. HER2 protein levels are normalized to GAPDH.

(F–M) Cells were pulsed with 150 μCi/mL [^{35}S]Met/Cys for 30 min, and immunoprecipitation for HER2 and immunoglobulin G (IgG) was performed.

(F and G) Phosphorimaging and liquid scintillation counts of radiolabeled HER2 in HCC1954-LCC1 cells treated with DMSO or 10 μM GNF5 for 48 h.

(H and I) Phosphorimaging and quantification of radiolabeled HER2 in ErbB2-BrM2 cells treated with DMSO or 10 μM GNF5 for 48 h.

(J and K) Phosphorimaging and liquid scintillation counts of radiolabeled HER2 in HCC1954-LCC1 cells virally transduced with shScr or shAA.

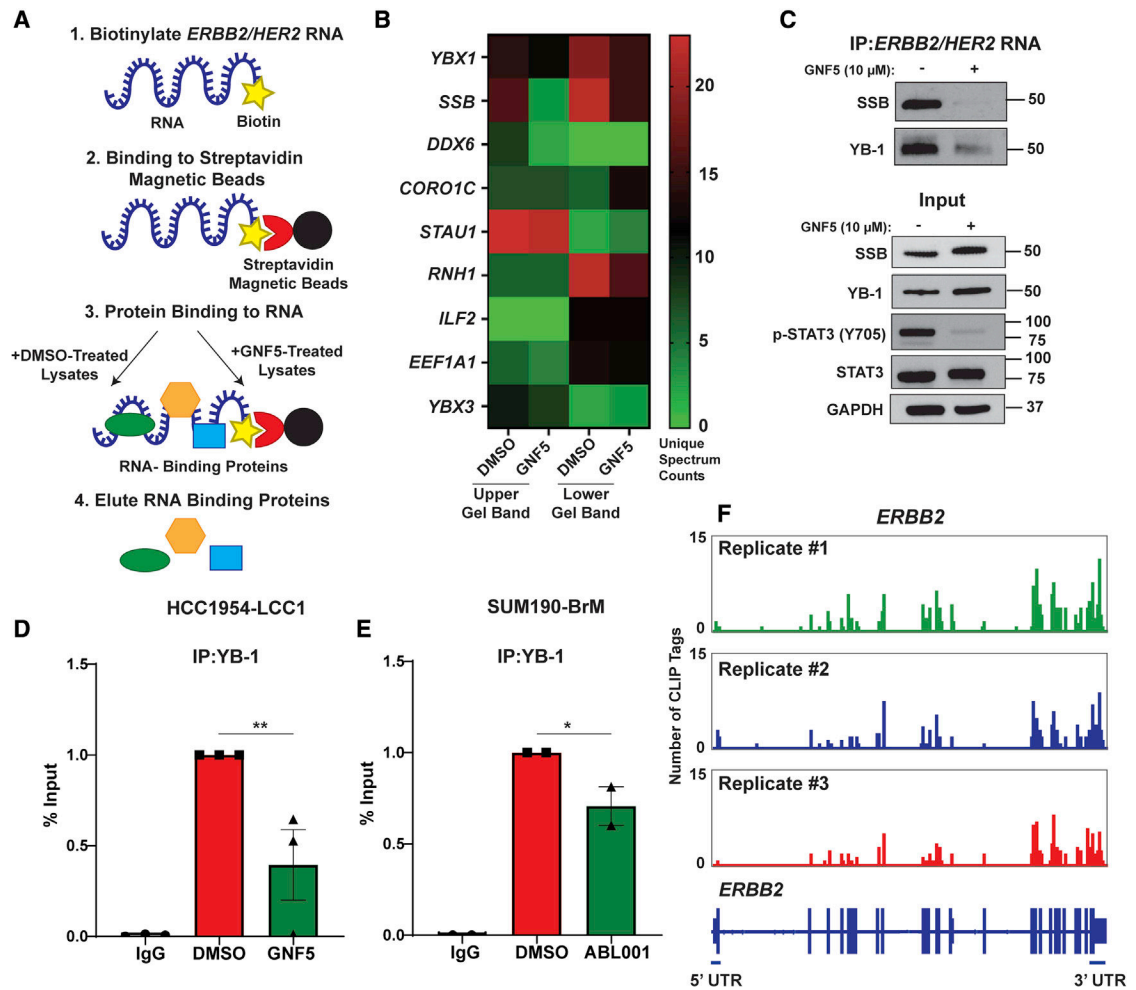(L and M) Phosphorimaging and liquid scintillation counts of radiolabeled HER2 in HCC1954-LCC1 cells treated with DMSO or 10 μM DPH for 48 h.

GAPDH was used as the housekeeping gene for qRT-PCR. Statistical analysis was performed using Student's t test and one-way ANOVA with Bonferroni's post hoc testing (n = 3). n.s., not significant, *p < 0.05, **p < 0.01, ***p < 0.001, ****p < 0.0001. Data are mean ± SEM.

Figure 4. ABL kinase inhibition disrupts *ERBB2* mRNA binding to Y-box-binding protein 1

(A) Workflow of RNA-binding protein pull-down. *ERBB2* mRNA was biotinylated, bound to streptavidin magnetic beads, and incubated with lysates from HCC1954-LCC1 cells treated with DMSO or 10 μM GNF5 for 48 h, and RNA-binding proteins were eluted.

(B) Heatmap of unique spectrum counts of eluted RNA-binding proteins from the coding region of *ERBB2* mRNA as identified by mass spectrometry analysis.

(C) Immunoblots of RNA-binding proteins SSB and YB-1 from the eluates of the *ERBB2* CDS mRNA binding protein pull-down. p-STAT3 serves as a marker of ABL kinase activity.

(D and E) RNA immunoprecipitation of YB-1 followed by qRT-PCR of *ERBB2* in HCC1954-LCC1 and SUM190-BrM cells. *ERBB2* mRNA levels were normalized to immunoprecipitation input.

(D) HCC1954-LCC1 cells were treated with DMSO or 10 μM GNF5 for 48 h.

(E) SUM190-BrM cells were treated with DMSO or 10 μM ABL001 for 72 h (n = 2).

(F) Mapped CLIP tags across whole *ERBB2* gene (bottom) from YB-1 CLIP-sequencing analysis for 3 biological replicates.

Statistical analysis was performed using a one-way ANOVA with Holm-Šidák post hoc testing (n = 3). *p < 0.05, **p < 0.01. Data are mean ± SEM
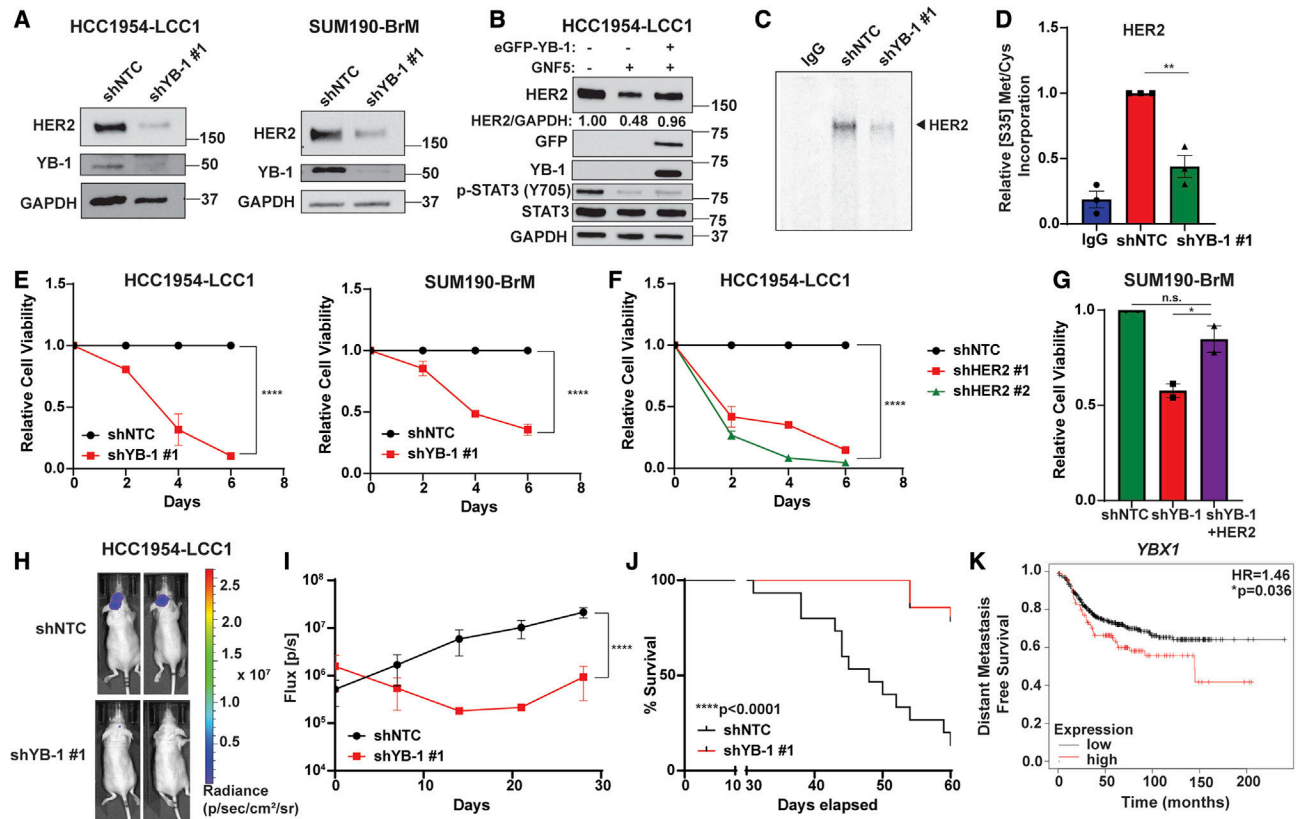
Figure 5. YB-1 knockdown decreases HER2 protein levels and inhibits outgrowth in the brain by HER2+ breast cancer cells

(A) Immunoblots of HER2 in HCC1954-LCC1 and SUM190-BrM cells transduced with shRNAs targeting YB-1 (shYB-1 #1) or a non-target control (shNTC).

(B) Immunoblots of HER2 in HCC1954-LCC1 transduced with TetO-FUW-pgk-puro empty vector or TetO-FUW-eGFP-YB-1-pgk-puro. Cells were treated with 1 μg/mL doxycycline and DMSO or 10 μM GNF5 for 48 h.

(C and D) Phosphorimaging of radiolabeled HER2 in HCC1954-LCC1 cells virally transduced with shNTC or shYB-1 #1 and pulsed with 150 μCi/mL [^{35}S]Met/Cys for 30 min. HER2 or IgG was immunoprecipitated. Liquid scintillation counts of immunoprecipitated HER2 were measured.

(E) Cell viability of HCC1954-LCC1 and SUM190-BrM cells virally transduced with shNTC or shYB-1 #1 as measured by CellTiter-Glo. All time points for shNTC were normalized to 1.

(F) Cell viability of HCC1954-LCC1 cells virally transduced with shNTC or shRNAs targeting HER2 (shHER2 #1, or shHER2 #2) as measured by CellTiter-Glo. All time points for shNTC were normalized to 1.

(G) Cell viability of SUM190-BrM cells virally transduced with shNTC or shYB1 #1 and empty vector or HER2 as measured by CellTiter-Glo (n = 2).

(H–J) Nude mice were injected intracranially with HCC1954-LCC1 cells transduced with shNTC (n = 15) or shYB-1 #1 (n = 15). Representative bioluminescent images of mice at day 28 are shown. BLI was monitored weekly to measure brain flux over time. Overall survival is shown. p/s, photons/second.

(K) Distant metastasis-free survival of patients with HER2+ breast cancer with high and low expression of *YBX1* is shown. Survival groups were separated by quartile based on mRNA expression (n = 451 total patients).

Statistical analysis was performed using a one-way ANOVA or repeated measures ANOVA with Bonferroni or Holm-Šídák post hoc testing (n = 3). For survival studies, statistical analysis was performed using a log rank (Mantel-Cox) test. n.s., not significant, $*p < 0.05$, $**p < 0.01$, $****p < 0.0001$. Data are mean ± SEM.

Figure 6. ABL1-mediated tyrosine phosphorylation of YB-1 is required for ERBB2 translation and HER2 protein expression

(A) Immunoprecipitation (IP) of FLAG and subsequent immunoblotting in HEK-293T cells were co-transfected with 3×FLAG-YB-1 and a hyperactive form of ABL1 (ABL1PP) (top).

(B) GFP IP and subsequent immunoblotting of HEK-293T cells co-transfected with EGFP-YB-1 and ABL1PP and treated with DMSO or 40 μM GNF5 for 24 h (top).

(C) coIP of GFP and subsequent immunoblotting of HEK-293T cells co-transfected with EGFP-YB-1 and ABL1PP (top).

(D) coIP of GFP and subsequent immunoblotting of HEK-293T cells co-transfected with EGFP-ABL1PP and 3×FLAG-YB-1 (top).

(E) GFP IP and subsequent immunoblotting of HCC1954-LCC1 cells virally transduced with N174-EGFP-YB-1 and transfected with ABL1PP (top).

(F) GFP IP and subsequent immunoblotting of SUM190-BrM N174 and N174-EGFP-YB-1 cells treated with DMSO or 10 μM ABL001 for 48 h (top).

(G) Immunoblotting of an *in vitro* kinase assay with purified His-YB-1 and GST-ABL1.

(H) Diagram of full-length EGFP-YB-1 and EGFP-tagged YB-1 domains: EGFP-A/P domain (amino acids 1–51), EGFP-cold-shock domain (CSD) (amino acids 52–129), and EGFP-C-terminal domain (C-term) (amino acids 130–324).

(I) coIP of GFP and subsequent immunoblotting of HEK-293T cells co-transfected with ABL1PP and either full-length EGFP-YB-1 or EGFP-YB-1 domains (top).

(J) GFP IP and subsequent immunoblotting of HEK-293T cells co-transfected with ABL1PP and EGFP-YB-1 domains (top).

(K and L) HCC1954-LCC1 breast cancer cells were virally transduced with the TetO-FUW-pgk-puro empty vector (TetO-FUW), TetO-FUW-eGFP-YB-1-pgk-puro (eGFP-YB-1), or TetO-FUW-eGFP-YB-1 Y72/99F-pgk-puro (eGFP-YB-1 Y72/99F). Cells were then transduced with shNTC or shYB-1 #1 and treated with 1 μg/mL doxycycline for 72 h.

(K) Immunoblots and quantification for HER2 are shown (top). EGFP-YB-1 expression and endogenous YB-1 were detected with anti-YB-1 antibody.

(L) Cells were pulsed with 150 μCi/mL [^{35}S]-Met/Cys for 30 min. HER2 or IgG was immunoprecipitated. Liquid scintillation counts of immunoprecipitated HER2 were measured (n = 3 for all conditions except LCC1 TetO-FUW shYB-1 #1, which has n = 2). Statistical analysis was performed using a one-way ANOVA followed by Bonferroni post hoc testing.

For IP experiments, whole-cell lysate (WCL) immunoblots are shown on the bottom. GAPDH was used as a loading control (bottom). *p < 0.05. Data are mean ± SEM.
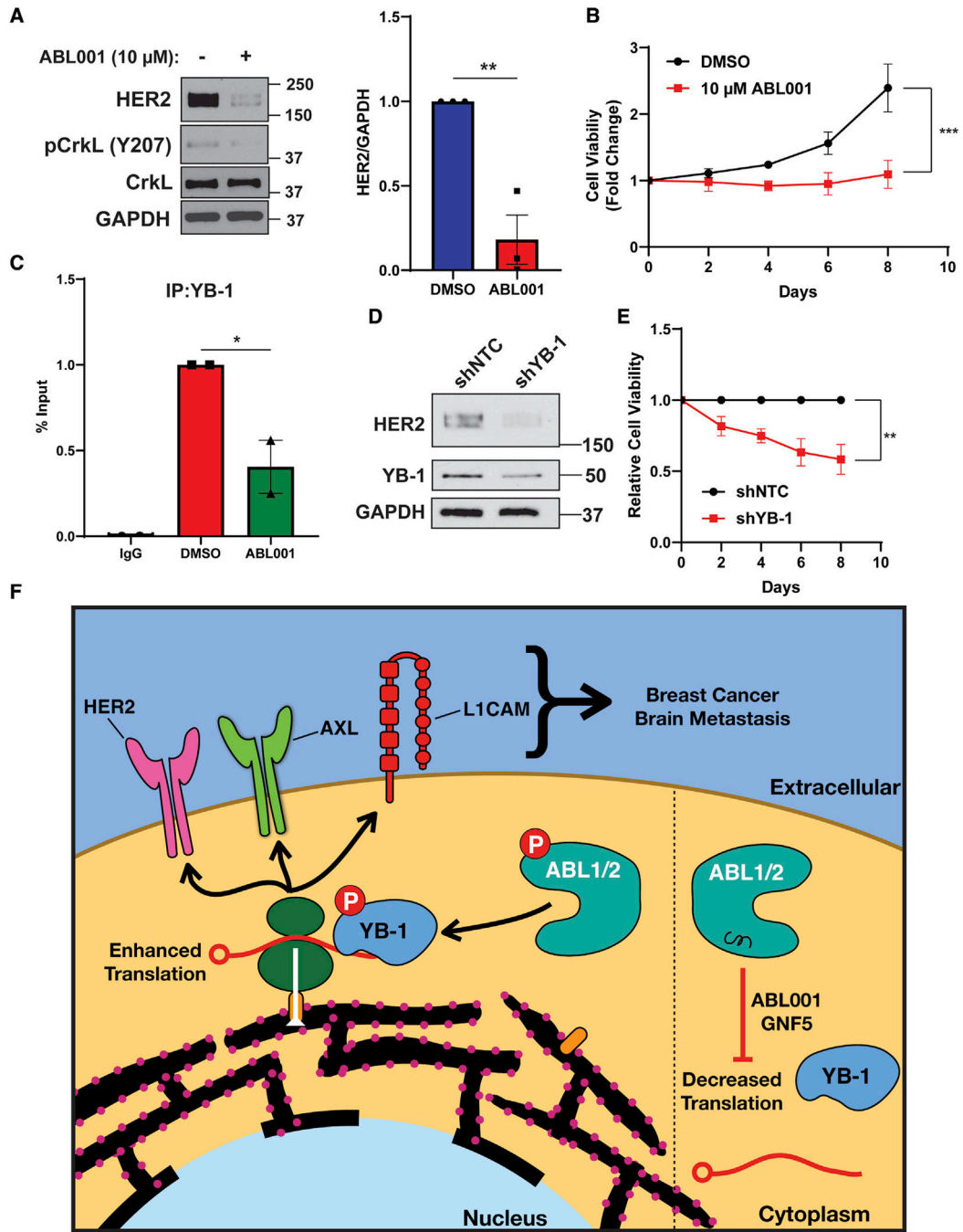
Figure 7. ABL inhibition and YB-1 knockdown reduces mutant HER2 protein in lung cancer cells

(A) HER2 immunoblot and quantification in NCI-H1781 cells treated with DMSO or 10 μM ABL001 for 72 h. p-CrkL is a marker of ABL kinase activity. HER2 protein quantifications were normalized to GAPDH.

(B) Cell viability of NCI-H1781 cells treated with DMSO or 10 μM ABL001 as measured by CellTiter-Glo.

(C) RNA IP of YB-1 followed by qRT-PCR to measure *ERBB2* mRNA in NCI-H1781 cells treated with DMSO or 10 μM ABL001 for 72 h. mRNA levels were normalized to IP input (n = 2).

(D) Immunoblot of HER2 in NCI-H1781 cells virally transduced with shNTC or shYB-1.

E) Cell viability of NCI-H1781 cells virally transduced with shNTC or shYB-1 as measured by CellTiter-Glo.

(F) Model diagram illustrating ABL-YB-1 signaling axis in HER2+ brain metastases.

Statistical analysis was performed using Student's t test, repeated measure ANOVA, and one-way ANOVA with Bonferroni post hoc testing (n = 3). *p < 0.05, **p < 0.01, ***p < 0.001. Data are mean ± SEM.

KEY RESOURCES TABLE

REAGENT or RESOURCE	SOURCE	IDENTIFIER
Antibodies		
HER2 (29D8)	Cell Signaling	Cat# 2165; RRID:AB_10692490
HER2 (D8F12)	Cell Signaling	Cat# 4290; RRID: AB_10557104
HER2 (3B5)	Santa Cruz	Cat# sc-33684; RRID:AB_627996
ABL1 (8×10^9)	BD Pharmingen	Cat# 554148; RRID:AB_2220994
Phospho-CrkL (Tyr207)	Cell Signaling	Cat# 3181; RRID:AB_331068
ABL2 (6D5)	Abnova	Cat# H00000027-M03; RRID: AB_565433
HER2 PE-Conjugated	R&D	Cat# FAB6744P; RRID: AB_10890577
Phospho-STAT3 (Tyr705)	Cell Signaling	Cat# 9145; RRID: AB_2491009
STAT3	Cell Signaling	Cat# 4904; RRID: AB_331269
CrkL (C-20)	Santa Cruz	Cat# sc-319; RRID:AB_631320
GAPDH (6C5)	Santa Cruz	Cat# sc-32233; RRID:AB_627679
APC/Fire 750 anti-human HER2	Biolegend	Cat# 324422; RRID: AB_2687225
SOX2	Cell Signaling	Cat#3579; RRID: AB_2195767
MMP9	Cell Signaling	Cat#13667; RRID: AB_2798289
Normal Mouse IgG	Santa Cruz	Cat# sc-2025; RRID: AB_737182
Normal Rabbit IgG	Novus Biologicals	Cat# NB810-56910; RRID: AB_844243
La antigen/SSB (D19B3)	Cell Signaling	Cat#5034; RRID: AB_10620954
YB-1 (59-Q)	Santa Cruz	Cat#sc-101198; RRID: AB_2219288
AXL (H-3)	Santa Cruz	Cat#sc-166269; RRID: AB_2243305
AXL (C89 $\times 10^7$)	Cell Signaling	Cat#8661; RRID: AB_11217435
SREBP1	Novus Biologicals	Cat# NB100-2215; RRID: AB_10002406
Phosphotyrosine (4G10)	Sigma	Cat#05-321; RRID: AB_309678
GFP (D5.1)	Cell Signaling	Cat#2956; RRID: AB_1196615
YB-1 (D2A11)	Cell Signaling	Cat#9744; RRID:AB_11178953
Phospho-ABL1 (Y245) (73×10^5)	Cell Signaling	Cat#2868; RRID:AB_2221094
FLAG M2 antibody	Sigma	Cat#F1804; RRID:AB_262044
TidyBlot Western Blot Detection Reagent:HRP	BioRad	Cat#STAR209P
Goat anti-Mouse IgG (H + L) Highly Cross-Adsorbed Secondary Antibody, Alexa Fluor 633	Thermo Fisher	Cat# A-21052, RRID: AB_2535719
NCAM-L1 (D5N9S)	Cell Signaling	Cat#89861, RRID: AB_2800145
Peroxidase AffiniPure Goat Anti-Mouse IgG (H + L)	Jackson Immunoresearch	Cat# 115-035-003, RRID:AB_10015289
Peroxidase AffiniPure Goat Anti-Rabbit IgG (H + L)	Jackson Immunoresearch	Cat#115-035-144
Chemicals, peptides, and recombinant proteins		
GNF-5 (Abl kinase small molecule inhibitor)	Duke Small Molecule Synthesis Facility	N/A
ABL001 (Asciminib)	Duke Small Molecule Synthesis Facility	N/A
EasyTag Express 35S Protein Labeling Mix	Perkin Elmer	Cat# NEG772007MC

REAGENT or RESOURCE	SOURCE	IDENTIFIER
Cycloheximide	Sigma	Cat#C6255
Actinomycin-D	Sigma	Cat#A9415
Anti asialo GM1 Rabbit	FUJIFILM Wako Chemicals	Cat#986-10001; RRID:AB_516844
Lenti-X Concentrator	Takara Bio	Cat #631231
DPH	Sigma	Cat #SML0202
GFP-Trap Agarose	Chromotek	Cat#gta-20
GST-ABL1 Recombinant Protein	Sino Biological	Cat#11199-H09B
His-YB1 Recombinant Protein	Novus Biologicals	Cat#NBP2-30101
Staurosporine	Sigma	Cat#S6942
Anti-FLAG M2 Affinity Gel	Sigma	Cat#A2220
PureLink RNase A	Thermo Fisher	Cat#12091021
Critical commercial assays		
Pierce Magnetic RNA-Protein Pull-Down Kit	Thermo Fisher	Cat# 20164
Pierce RNA 3′ End Desthiobiotinylation Kit	Thermo Fisher	Cat# 20163
Pierce Silver Stain for Mass Spectrometry	Thermo Fisher	Cat# 24600
MagnaRIP RNA-Binding Protein Immunoprecipitation Kit	Sigma	Cat#17-700
Cell Titer Glo	Promega	Cat# G7571
Hoescht 33342 Solution	Thermo Fisher	Cat# 62249
Caspase-Glo 3/7 Assay	Promega	Cat#G8091
Deposited data		
HER2 mRNA Binding Protein Pulldown Mass Spectrometry Data	This paper	MassIVE: MSV000087674
Original, Unprocessed Data	This paper	Mendeley Data: https://doi.org/10.17632/nzsk26yf5x.1
YB-1 HITS-CLIP dataset for long RNA species	Goodarzi et al., 2015	GEO: GSE63604
Metastatic Breast Cancer Project dataset	Metastatic Breast Cancer Project	cBioPortal
INSERM Metastatic Breast Cancer dataset	Lefebvre et al., 2016	EGA: EGAS00001001695
TCGA Breast Invasive Carcinoma dataset	TCGA, Firehose Legacy	cBioPortal
Sanger Breast Invasive Carcinoma dataset	Stephens et al., 2012	EGA: EGAD00001000133
Broad Breast Invasive Carcinoma dataset	Banerji et al., 2012	dbGaP: phs000369.v1.p1
British Columbia Breast Invasive Carcinoma dataset	Shah et al., 2012	EGA: EGAS00001000132
SMC Breast Cancer dataset	Kan et al., 2018	GEO: GSE113184
MSKCC Breast Cancer dataset	Nixon et al., 2019	cBioPortal
METABRIC Breast Cancer dataset	Curtis et al., 2012; Pereira et al., 2016	EGA: EGAS00001001753; EGAS00000000083
MSK Breast Cancer dataset	Razavi et al., 2018	dbGaP: phs001674.v1.p1
Experimental models: Cell lines		
HCC1954-LCC1	Malladi et al., 2016	N/A
ErbB2-BrM2	Valiente et al., 2014	N/A
SUM190-BrM	Gril et al., 2018	N/A

REAGENT or RESOURCE	SOURCE	IDENTIFIER
NCI-H1781	ATCC	Cat# CRL-5894; RRID: CVCL_1494
HEK-293T	ATCC	Cat# CRL-3216; RRID: CVCL_0063
Experimental models: Organisms/strains		
Outbred athymic nu/nu mice	Jackson Laboratory	Cat#007850; RRID: IMSR_JAX:007850
FVB/NJ	Jackson Laboratory	Cat#001800; RRID: IMSR_JAX:001800
Oligonucleotides		
See Table S4 for a list of all primers and oligonucleotides		
pLKO-puro Non-Target shRNA Control	Sigma Mission TRC1	SHC016-1EA
pLKO-puro shAGO1	Sigma Mission TRC1	TRCN0000007861
pLKO-puro shAGO2	Sigma Mission TRC1	TRCN0000007865
pLKO-puro shAGO3	Sigma Mission TRC1	TRCN0000007870
pLKO-puro shAGO4	Sigma Mission TRC1	TRCN0000007875
pLKO-puro shAGO4	Sigma Mission TRC1	TRCN0000007874
pLKO-puro shYB1 #1	Sigma Mission TRC1	TRCN0000007951
PLKO-puro shYB1 #2	This paper	N/A
pLKO-puro shYB1 #3	Sigma Mission TRC1	TRCN0000007948
pLKO-puro shSSB	Sigma Mission TRC1	TRCN0000062197
pLKO-puro shHER2	Sigma Mission TRC1	TRCN0000010341
pLKO-puro shHER2	Sigma Mission TRC1	TRCN0000010342
pLKO-puro shAXL #1	Sigma Mission TRC1	TRCN0000000572
pLKO-puro shAXL #2	Sigma Mission TRC1	TRCN0000000573
pLKO-puro shL1CAM #1	Sigma Mission TRC1	TRCN0000063913
pLKO-puro shL1CAM #2	Sigma Mission TRC1	TRCN0000063914
Scramble control shRNA	Gu et al., 2016	N/A
ABL1 shRNA	Gu et al., 2016	N/A
ABL2 shRNA	Gu et al., 2016	N/A
pBABEpuro-ERBB2	Greulich et al., 2012	Addgene #40978; RRID: Addgene_40978
lentiCas9-Blast	Sanjana et al., 2014	Addgene #52962; RRID: Addgene_52962
LentiGuide-Hygro	http://n2t.net/addgene:139462	Addgene #139462; RRID: Addgene_139462
LentiGuide-Neo	Doyle et al., 2018	Addgene #139449; RRID: Addgene_139449
LentiGuide-Puro	Sanjana et al., 2014	Addgene #52963; RRID: Addgene_52963
LentiGuide-sgRNA human ABL1 #1-Neo	This paper	N/A
LentiGuide-sgRNA human ABL1 #2-Neo	This paper	N/A
LentiGuide-sgRNA human ABL2 #1-Hygro	This paper	N/A
LentiGuide-sgRNA human ABL2 #2-Hygro	This paper	N/A
LentiGuide-sgRNA mouse ABL1 #1-Hygro	This paper	N/A
LentiGuide-sgRNA mouse ABL2 #1-Puro	This paper	N/A
pLVX-Tet-On Advanced	Clontech	Ref# 632162

REAGENT or RESOURCE	SOURCE	IDENTIFIER
TetO-FUW-pgk-puro	Chowdhury et al., 2016	Addgene #85747; RRID: Addgene_85747
TetO-FUW-HER2-pgk-puro	This paper	N/A
pcDNA-ABL1PP	Plattner et al., 2004	N/A
pcDNA-ABL2PP	Plattner et al., 2004	N/A
mEGFP-c1	http://n2t.net/addgene:54759	Addgene #54759; RRID: Addgene_54759
mEGFP-YB1-c1	This paper	N/A
pcDNA-GFP-ABL1	Burton et al., 2003	N/A
GFP-ABL1PP	This paper	N/A
mEGFP-YB1 A/P Domain-c1	This paper	N/A
mEGFP-YB1 CSD-c1	This paper	N/A
mEGFP-YB1 CSD Y72F-c1	This paper	N/A
mEGFP-YB1 CSD Y99F-c1	This paper	N/A
mEGFP-YB1 C-Term Domain-c1	This paper	N/A
3xFLAG-FUS-WT	Yamazaki et al., 2012	Addgene #44985; RRID: Addgene_44985
3xFLAG-YB-1	This paper	N/A
N174-MCS	http://n2t.net/addgene:81061	Addgene #81061; RRID: Addgene_81061
N174-eGFP-YB-1-MCS	This paper	N/A
perbB2-ECFP	Offterdinger and Bastiaens, 2008	Addgene #40268; RRID: Addgene_40268
pDESTmycYBX1	Landthaler et al., 2008	Addgene #19878; RRID: Addgene_19878
Software and algorithms		
Prism 8	Graphpad	http://graphpad.com/scientific-software/prism
ImageJ	Schneider et al., 2012	http://imagej.nih.gov
Living Image	Perkin Elmer	http://perkinelmer.com
CLIP Tool Kit	Shah et al., 2017	https://zhanglab.c2b2.columbia.edu/index.php/CTK_Documentation